

1 **Supporting Information for “Body mass – biomass scaling modulates**
2 **species keystone-ness to press perturbations”**

3 Xiaoxiao Li, Wei Yang, Mark Novak, Lei Zhao, Peter C. de Ruiter, Zhifeng Yang, Christian
4 Guill

5

6 **Table of Contents:**

- 7 • **Appendix S1. Sensitivity on diagonal elements of the community matrices**
8 **of empirical food webs**
- 9 • **Appendix S2. Extension from the original ATN model to the updated ATN**
10 **model**
- 11 • **Appendix S3. Parameters used to generate bottom-heavy or top-heavy**
12 **biomass-distributed food webs**
- 13 • **Appendix S4. Predefined criteria to filter simulations**
- 14 • **Appendix S5. Deriving community matrix for model food webs**
- 15 • **Appendix S6. Comparison between the normalized inverse community**
16 **matrix and the inverse community matrix**
- 17 • **Supplementary Tables: Tables S1–S7**
- 18 • **Supplementary Figures: Figs. S1–S11**
- 19 • **Supplementary References**

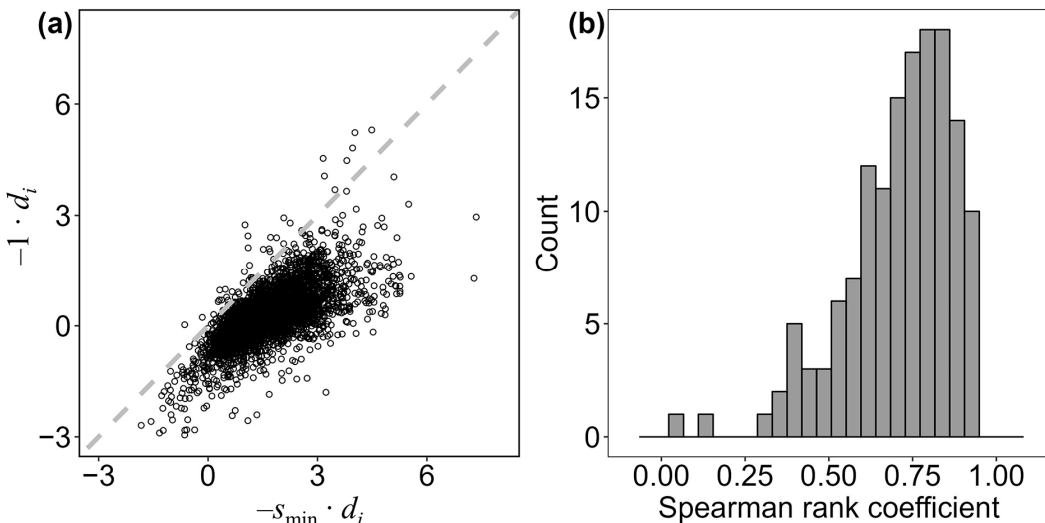
20 **Appendix S1. Sensitivity on diagonal elements of the community**
21 **matrices of empirical food webs**

22 The approach of normalized inverse community matrix assumes that the system is at
23 equilibrium (Bender et al. 1984). To meet this assumption, we ensured that each empirical food
24 web's community matrix \mathbf{A} has a negative real part for its leading eigenvalue by adjusting its
25 diagonal elements. Following Neutel et al. (2002), we determined the minimum value of s
26 (where $0 < s < 1$) required to stabilize the matrix, calculated as $-s_{\min} \cdot d_i$, where d_i is the specific
27 death rate of species i . This adjustment produced conservatively stable food webs. To explore
28 the potential impact, we conducted an additional analysis using a less conservative assumption
29 by replacing $-s_{\min} \cdot d_i$ with $-1 \cdot d_i$, resulting in more negative eigenvalues and thus, a more
30 stable configuration for the empirical food webs (de Ruiter et al. 1995).

31 Quantitatively, we found that species' per capita net effects were generally higher with $-s_{\min} \cdot$
32 d_i in the diagonal compared to predictions using $-1 \cdot d_i$ (**Fig. A1.1a**). This is expected as higher
33 absolute values of the diagonal elements mean stronger self-limitation, and intuitively, a species
34 that is strongly self-limited (e.g., by availability of nesting sites or heavy parasite load) will not
35 respond much if its predators, prey, or competitors become more or less abundant. This finding
36 is consistent with Nakajima (1992) and Novak et al. (2016), suggesting that more stable food
37 webs exhibit less pronounced effects under press perturbations. We further examined the
38 Spearman rank correlation between the two sets of predictions of species' per capita net effects
39 within each food web. The results showed that, in most cases, the predictions were highly
40 correlated, with an interquartile range of Spearman rank correlation coefficients from 0.61 to
41 0.83 (**Fig. A1.1b**). That said, there were two individual food webs (of the 144 webs in total)
42 that showed notably weak correlations, with coefficients of 0.05 and 0.16, potentially due to
43 low species richness (**Fig. A1.2**).

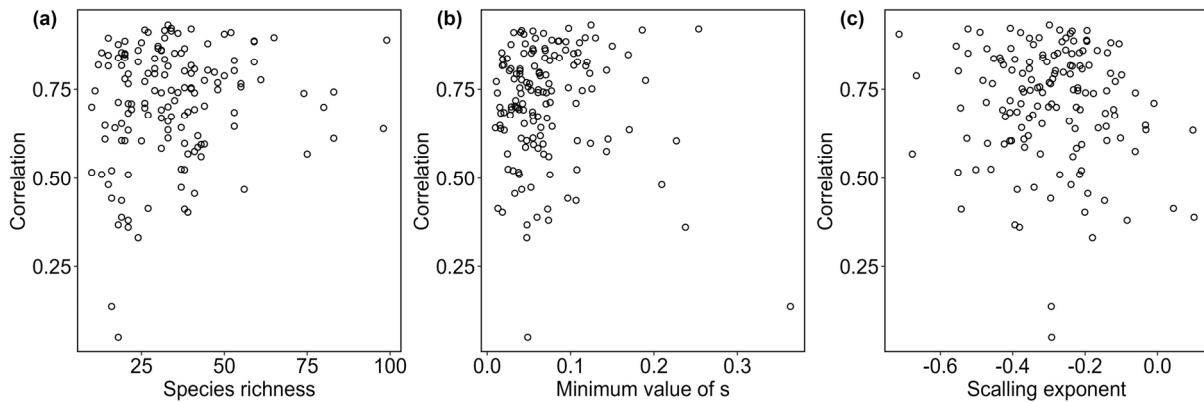
44 This analysis suggests that while the assumption of a minimum s value contributes to
45 conservative stability, the overall qualitative predictions of species keystone-ness remain robust
46 across different s values. However, the influence of uncertainty in the diagonal elements on
47 predictions from the normalized inverse community matrix warrants further investigation, as
48 this uncertainty has been found to potentially impact qualitative predictions (Iles & Novak 2016;
49 Koslicki & Novak 2018; Novak et al. 2011).

50



51 **Fig. A1.1** (a) Comparison of species' per capita net effects estimated using two different assumptions
 52 regarding the diagonal elements of community matrices: $-s_{\min} \cdot d_i$ (x-axis) and $-1 \cdot d_i$ (y-axis). The dashed
 53 line represents the 1:1 line. (b) Histogram of Spearman rank correlation coefficient between the two sets of
 54 predictions across empirical food webs.

55



56

57 **Fig. A1.2** Spearman rank correlation coefficients between species' per capita net effects estimated from two
 58 different assumptions in the diagonal elements: $-s_{\min} \cdot d_i$ and $-1 \cdot d_i$, across empirical food webs, shown as a
 59 function of (a) species richness, (b) minimum value of s , (c) scaling exponents of species' body mass to
 60 biomass.

61 **Appendix S2. Extension from the original ATN model to the updated ATN
62 model**

63 The Allometrical Trophic Network (ATN) model (Yodzis & Innes 1992), based on the metabolic
64 theory of ecology, correlates biological rates with body mass to predict metabolic activity from
65 the individual to the community level (Brown et al. 2004). In the original ATN model (e.g.,
66 Brose et al. 2006; Schneider et al. 2016; Yodzis & Innes 1992), the dynamics of consumer
67 biomass (B_j) are typically expressed as follows:

68
$$\frac{dB_j}{dt} = eB_j \sum_i g_{ij} - \sum_n B_n g_{jn} - x_j B_j \quad (\text{S1})$$

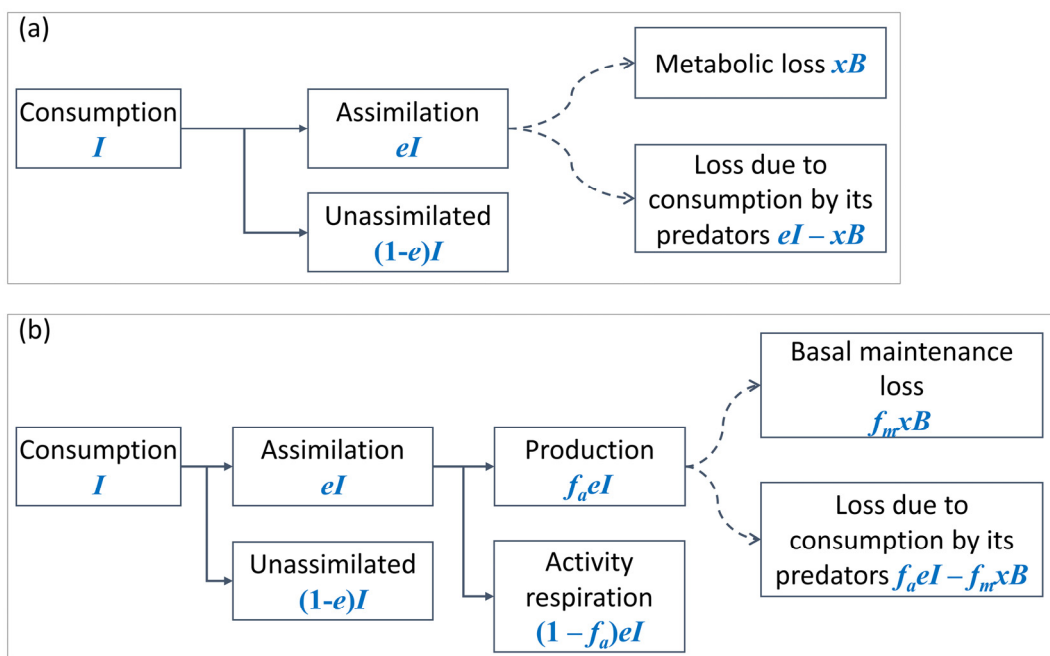
69 where e represents the assimilation efficiency, usually 0.45 for herbivores and 0.85 for
70 carnivores, reflecting the quality and stoichiometry of their respective food sources. x_j is the
71 mass-specific metabolic rate of consumer j , and g_{ij} is the functional response. In this original
72 ATN model, the assimilated energy is allocated either to metabolic loss (i.e., basal respiration)
73 or to loss due to consumption by its predators (**Fig. A2.1a**).

74 However, this setup does not account for activity respiration, which is the energy spent for
75 processes related to the production of new biomass (including locomotion, foraging, food
76 handling and digestion, ontogenetic processes, and reproduction), proportional to the amount
77 of assimilated energy. While the energetic structure of the original ATN model may be suitable
78 for homoiothermic (warm-blooded) animals like mammals and birds with high basal respiration
79 (basic bodily functions), it is less appropriate for pelagic ecosystems dominated by unicellular
80 organisms and invertebrates, which tend to have low basal respiration but high activity
81 respiration linked to food uptake (Anderson 1992). In the original ATN model (without activity
82 respiration) trophic transfer efficiencies (ratio of production at two adjacent trophic levels) can
83 be unrealistically high (Kath et al. 2018).

84 In response to these limitations, studies like Boit et al. (2012) and Kath et al. (2018) extended
85 the original ATN model to separately account for basal and activity respiration, resulting in a
86 more realistic simulation of trophic energy flows (Martinez 2020). The biomass dynamics of
87 consumers are now described as:

88
$$\frac{dB_j}{dt} = f_a eB_j \sum_i g_{ij} - \sum_n B_n g_{jn} - f_m x_j B_j \quad (\text{S2})$$

where f_a is the fraction of assimilated carbon allocated to production, with $(1-f_a)$ representing the fraction lost to activity respiration. f_m is the fraction of basal maintenance loss relative to total metabolic loss. It is analog to the basal metabolic rate defined for homiotherms (Gessaman 1973) as measured in the thermoneutral zone where homiotherms have very low costs for thermoregulation and are most similar to ectotherms in this regard (Kath et al. 2018). Thus, the assimilated energy in the updated ATN mode is divided as follows: (1) Activity respiration; (2) Basal maintenance loss; (3) Loss due to consumption by its predators (Fig. A2.1b).



97

Fig. A2.1 Structure of (a) the original allometric trophic network model, as defined in studies like Yodzis & Innes (1992) and Brose et al. (2006), and (b) the updated model used in our study and studies such as Boit et al. (2012) and Kath et al. (2018). Solid arrows represent energy flows, while dashed arrows indicate biomass dynamics.

102 Compared to the original ATN model, in the updated ATN model $f_a \cdot e$ represents production
 103 efficiency (functioning equivalent to e in the original model), and $f_m \cdot x$ represents the per
 104 capita basal maintenance loss rate (functioning equivalent to x in the original model). In the
 105 original ATN model, $f_a = f_m = 1$. In both Boit et al. (2012) and Kath et al. (2018), the parameters
 106 $f_a = 0.4$ and $f_m = 0.1$ were used. While this assumption already introduces more realistic trophic
 107 transfer efficiencies than the original ATN model (Kath et al. 2018), we found it still often
 108 results in top-heavy food webs and struggles to produce bottom-heavy structures (cf. Fig. A3.1a
 109 in Appendix S3). Hence, we introduce another scenario that uses different values of f_a : $f_a = 0.4$

110 for herbivores (written as f_R) and $f_a = 0.05$ for carnivores (written as f_C), referring to the values
111 of production efficiency normally assumed in L-V models (Heal and MacLean 1975), meaning
112 that herbivores allocate a higher proportion of assimilated energy to production, while
113 carnivores allocate more to activity respiration likely due to the mobility of its prey. The latter
114 scenario lowers the trophic transfer efficiency of carnivorous consumers, enabling the
115 generation of more bottom-heavy food webs (cf. **Fig. A3.1b**).

116 **Appendix S3. Parameters used to generate bottom-heavy or top-heavy**
117 **biomass-distributed food webs**

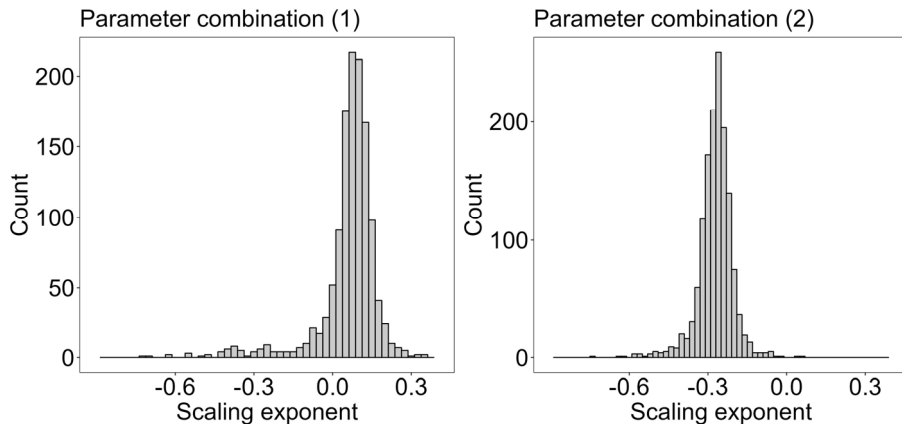
118 We used two combinations of the factors related to trophic transfer efficiency (f_R , f_C , f_m , see
119 **Appendix S2**), along with different mass scaling exponents of attack rates (β_i and β_j , see **Table**
120 **1**) and handling times (η_i and η_j , see **Table 1**), to regulate how biomass scales from smaller to
121 larger species.

122 In the first parameter combination (**Table 1**), the fraction of assimilated energy used for
123 production was set to 0.4 for both herbivores (f_R) and carnivores (f_C) (i.e., $f_R = f_C = 0.4$), and the
124 fraction for basal maintenance loss f_m assumed as 0.1 following Boit et al. (2012) and Kath et
125 al. (2018). The exponents β_i and β_j of attack rates were drawn from normal distributions with
126 means of 0.15 and 0.47, respectively, and the exponents η_i and η_j of handling times were
127 sampled from normal distributions with means of -0.66 and -0.48 , respectively, referring to
128 the established empirical model based on various species, including ectotherm vertebrates,
129 invertebrates, and unicells in both freshwater and marine ecosystems (Rall et al. 2012). We
130 assumed a constant $m_i^{\beta_i} = 20$ for plant resources (**Table 1**), as plants are immobile, and a
131 constant $a_0 = 50$ for all capture coefficients, following Schneider et al. (2016).

132 In the second parameter combination (**Table 1**), we assumed $f_R = 0.4$ for herbivores and $f_C =$
133 0.05 for carnivores, meaning that herbivores allocate a higher proportion of assimilated energy
134 to production, while carnivores allocate more to activity respiration due to the mobility of its
135 prey. The exponents β_i and β_j were drawn from normal distributions with means of 0.09 and
136 0.85, respectively, and the exponents η_i and η_j were sampled from normal distributions with
137 means of -0.24 and -0.76 , respectively, referring to the established empirical model solely
138 based on marine invertebrate species (Rall et al. 2012), to better align with our empirical food
139 webs. We assumed a constant $m_i^{\beta_i} = 1$ for plant resources and a constant $a_0 = 10$ following
140 Ryser et al. (2021).

141 For each parameter combination, we conducted 2,500 simulations across a gradient of initial
142 species richness, ranging from 20 to 100 in steps of 20, and performed 500 replicates for each
143 richness level. Simulations were filtered based on equilibrium biomasses and final trophic
144 structure according to predefined criteria (cf. **Appendix S4**). This resulted in 1,367 and 1,432
145 accepted model food webs for parameter combinations (1) and (2), respectively. The first
146 parameter combination typically produced top-heavy food webs, while the second tended to

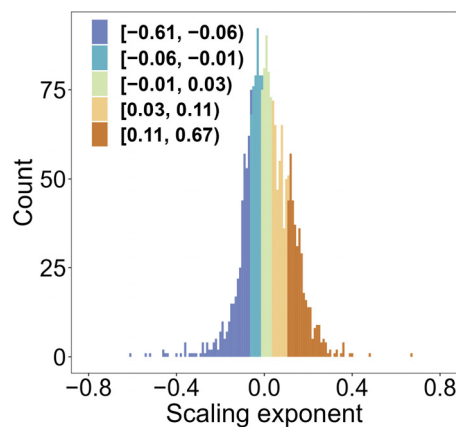
147 produce bottom-heavy food webs (see **Fig. A3.1**), leading to the bimodal distribution of scaling
148 exponents of all accepted model food webs shown in **Fig. 1b**.



149
150 **Fig. A3.1** Histograms of the scaling exponent of species' body mass to biomass across model food webs
151 generated using different parameter combinations.

152 • Sensitivity analysis on factors f_R , f_C , and f_m

153 We repeated the initial 5,000 simulations (5 initial richness levels \times 500 replicates \times 2 parameter
154 combinations) from the main analyses, but this time using the original ATN model setup, where
155 $f_R = f_C = f_m = 1$. After completing all four steps of the filtering process (cf. **Appendix S4**), we
156 obtained 2,799 model food webs for the updated ATN model, representing both bottom-heavy
157 and top-heavy food webs (**Fig. 1b**). In contrast, using the original ATN model setup, we
158 obtained 1,991 model food webs after filtering, with scaling exponents of species' body mass
159 to biomass ranging from -0.61 to 0.67 (**Fig. A3.2**). The bottom-heavy food webs observed with
160 the updated ATN model setup were less likely to occur with the original ATN model setup.
161 Instead, a larger proportion of model food webs exhibited scaling exponents closer to zero, with
162 the interquartile range from -0.05 to 0.08 , and a higher likelihood of positive scaling exponents.



163
164 **Fig. A3.2** Histogram of scaling exponent of species' body mass to biomass across model food webs generated

165 under the original ATN model setup ($n = 1,991$ model food webs).

166 • Sensitivity analysis on mass scaling exponents β_i , β_j , η_i , and η_j

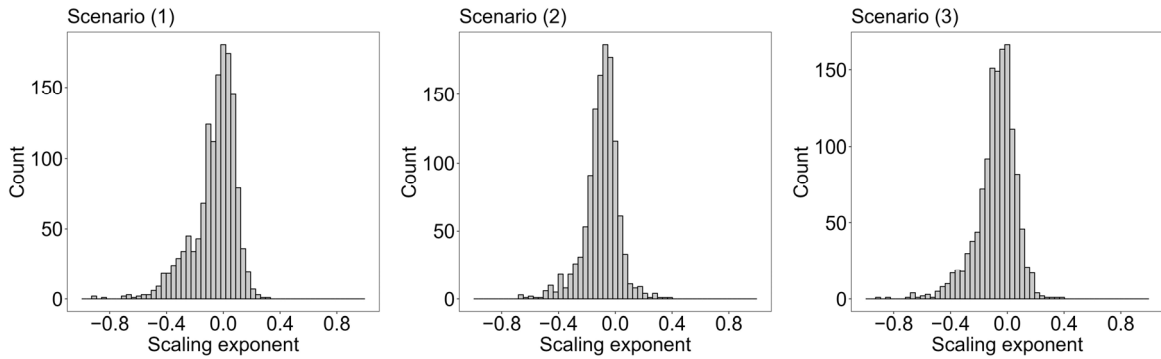
167 We ran simulations with randomly selected parameter values, except that f_R was set to 0.4 and
168 f_m was set to 0.1. Specifically, f_C was randomly selected from a uniform distribution between
169 0.05 and 0.4; a_0 was randomly selected from a uniform distribution between 10 and 50 (**Table**
170 **1**); If species i is a basal species, $m_i^{\beta_i}$ was randomly selected from a uniform distribution
171 between 1 and 20. The body mass scaling exponents used in the attack rates and handling times
172 differ across the following three scenarios:

173 Scenario (1): $\beta_i \sim N(\mu = 0.15, \sigma = 0.05)$ and $\beta_j \sim N(\mu = 0.47, \sigma = 0.05)$; $\eta_i \sim N(\mu = -0.66, \sigma = 0.02)$
174 and $\eta_j \sim N(\mu = -0.48, \sigma = 0.03)$;

175 Scenario (2): $\beta_i \sim N(\mu = 0.09, \sigma = 0.05)$ and $\beta_j \sim N(\mu = 0.85, \sigma = 0.05)$; $\eta_i \sim N(\mu = -0.24, \sigma = 0.02)$
176 and $\eta_j \sim N(\mu = -0.76, \sigma = 0.03)$;

177 Scenario (3): Parameters were randomly selected either from the set in Scenario (1) or from the
178 set in Scenario (2).

179 For each scenario, we initially ran 2,500 simulations with randomly selected parameter values
180 across five levels of initial species richness, ranging from 20 to 100 in steps of 20, and
181 performed 500 replicates for each richness level. We then filtered these simulations based on
182 the predefined criteria outlined in **Appendix S4**. We compared the histogram distributions of
183 the scaling exponents of species' body mass to biomass for the accepted model food webs across
184 the three scenarios (**Fig. A3.3**). We observed that the majority of food webs generated under
185 these random parameters tend to have scaling exponents clustered close to zero, indicating an
186 invariant distribution of biomass with increasing body mass or trophic level. While the
187 interquartile range of scaling exponents for Scenario (2) shifted more towards negative values,
188 fixing the mass scaling exponents in the attack rates and handling time using established values
189 based on several organisms in freshwater and marine ecosystems or only using the marine
190 invertebrate species had little impact on the resulting community biomass structure.



191

192 **Fig. A3.3** Histograms of the scaling exponent of species' body mass to biomass across model food webs
 193 generated under the three scenarios. The scaling exponents of the accepted model food webs range from
 194 -0.91 to 0.30 for scenario (1) ($n = 1,385$ food webs), from -0.67 to 0.37 for scenario (2) ($n = 1,190$ food
 195 webs), and from -0.89 to 0.37 for scenario (3) ($n = 1,283$ food webs).

196 **Appendix S4. Predefined criteria to filter simulations**

197 Initially, we generated 5,000 model food webs, accounting for 5 initial species richness levels
198 \times 500 replicates \times 2 parameter combinations. Using the equilibrium biomasses and the final
199 trophic structure, we applied predefined criteria to filter simulations, selecting only those cases
200 that displayed sufficient complexity and reached a stable equilibrium state characterized by the
201 leading eigenvalue with a negative real part of the resulting community matrix.

202 The exclusion criteria were as follows: (1) the minimum number of persistent species must be
203 greater than 5; (2) the maximum trophic level of consumers must not be below 3 and not higher
204 than 6; (3) the absolute value of species per-capita growth rate over the evaluation period should
205 not exceed 1% of their metabolic rate to remove strong temporary fluctuations; and (4) the
206 resulting community matrix has a leading eigenvalue with a negative real part to ensure the
207 model food web reached a stable equilibrium.

208 In the end, we obtained 2,799 food webs—accounting for 56% of the initial setups—for further
209 analysis.

210 **Appendix S5. Deriving community matrix for model food webs**

211 For each accepted model food web, we derived its community matrix \mathbf{A} when its simulation
 212 reached a stable equilibrium. The diagonal elements of \mathbf{A} reflect the per capita self-effects. For
 213 basal species, this was expressed as

$$214 \quad \alpha_{ii} = \frac{\partial \left(\frac{dB_i}{dt} \right)}{\partial B_i} = r_i G_i - \sum_j B_j \frac{\partial g_{ij}}{\partial B_i} - f_m x_i \quad (\text{S3}),$$

215 The consumer it was expressed as

$$216 \quad \alpha_{jj} = \frac{\partial \left(\frac{dB_j}{dt} \right)}{\partial B_j} = fe \sum_i g_{ij} + fe B_j \sum_i \frac{\partial g_{ij}}{\partial B_j} - \sum_n B_n \frac{\partial g_{jn}}{\partial B_j} - f_m x_j \quad (\text{S4}),$$

217 where fe is $f_R \cdot e_R$ when i is a basal species, otherwise $f_C \cdot e_C$ when i is an animal species.

218 The per-capita top-down effect of a predator j on its prey i is expressed as

$$219 \quad \alpha_{ij} = \frac{\partial \left(\frac{dB_i}{dt} \right)}{\partial B_j} = -g_{ij} - \frac{\partial g_{ij}}{\partial B_j} B_j \quad (\text{S5}),$$

220 The per-capita bottom-up effect of a prey i on its consumer j is expressed as

$$221 \quad \alpha_{ji} = \frac{\partial \left(\frac{dB_j}{dt} \right)}{\partial B_i} = fe B_j \frac{\partial g_{ij}}{\partial B_i} \quad (\text{S6}),$$

222 where fe is $f_R \cdot e_R$ when i is a basal species, otherwise $f_C \cdot e_C$ when i is an animal species.

223 $\frac{\partial g_{ij}}{\partial B_i}$ and $\frac{\partial g_{ij}}{\partial B_j}$ are derivatives of the consumer's functional response:

$$224 \quad \frac{\partial g_{ij}}{\partial B_i} = \frac{\partial \left(\frac{w_j a_{ij} B_i^q}{1 + \sum_l c_{lj} B_l + w_j \sum_{k \in \text{prey}} h_{kj} a_{kj} B_k^q} \cdot \frac{1}{m_j} \right)}{\partial B_i} = \frac{q g_{ij}}{B_i} - \frac{(g_{ij})^2 m_j (c_{ij} + w_j a_{ij} h_{ij} q B_i^{q-1})}{w_j a_{ij} B_i^q} \quad (\text{S7}),$$

225

$$\frac{\partial g_{ij}}{\partial B_j} = \frac{\partial}{\partial B_j} \left(\frac{w_j a_{ij} B_i^q}{1 + \sum_l c_l B_l + w_j \sum_{k \in \text{prey}} h_{kj} a_{kj} B_k^q} \cdot \frac{1}{m_j} \right) = \left(g_{ij} \right)^2 \frac{-m_j c_{jj}}{w_j a_{ij} B_i^q} \quad (\text{S8}).$$

226 All parameters are shown in **Table 1**.

227 **Appendix S6. Comparison between the normalized inverse community**
228 **matrix and the inverse community matrix**

229 In our study, each element in the community matrix \mathbf{A} represents the direct effect (both top-
230 down and bottom-up) of species j on the population growth rate of species i (see Eq. 1-2 for
231 empirical food webs and Eq. S3-S6 for model food webs) with all other species held constant.
232 Therefore, each element in the inverse community matrix \mathbf{A}^{-1} (y_{ij}) indicates how the equilibrium
233 biomass of the species in row i is expected to respond to a unit change in the population growth
234 rate of the species in column j , considering all direct and indirect interactions between the two
235 species (Yodzis 1988).

236 The normalized inverse community matrix $\tilde{\mathbf{A}}^{-1}$ is further derived by dividing each column of
237 the inverse community matrix by its diagonal element (Novak et al. 2016). Each element in
238 $\tilde{\mathbf{A}}^{-1}$ (\tilde{y}_{ij}) represents how the equilibrium biomass of species i adjusts relative to a perturbation-
239 induced change in the biomass of species j . Consequently, this normalized matrix enables us to
240 determine species keystone-ness on a per capita basis. The off-diagonal elements in each
241 column of $\tilde{\mathbf{A}}^{-1}$ can be summed to understand the joint effects of a perturbation-induced change
242 in perturbed species in the column on all other species, defined as species' *per capita net effect*.
243 Corresponding to the linear approximation of the per capita net effect, the nonlinear responses
244 of species' *per capita community biomass* change resulting from species-specific press

245 perturbations is calculated as $\sum_{i=1}^S \left| \frac{B_i^{post} - B_i^{pre}}{B_j^{post} - B_j^{pre}} \right|$, where B^{pre} and B^{post} denote the equilibrium
246 biomass of the species before and after perturbation.

247 To determine whether the per capita effects were pivotal to our findings, we evaluated the total
248 net effects of species and calculated the corresponding total community biomass change for
249 each species-specific press perturbation. Following the methodology of previous studies (Berg
250 et al. 2011; Montoya et al. 2009), the *total net effect* that species j has on all other species within
251 the food web is quantified by summing the absolute values of the elements in the species'
252 column within \mathbf{A}^{-1} , without normalization, excluding the diagonal element. Species' total net
253 effect represents the joint effect of a unit change in the population growth rate of the perturbed
254 species on the equilibrium biomasses of all other species. Regarding our applied species-
255 specific press perturbations, the corresponding *total community biomass change* for a species

related to their *total net effect* can be quantified as $\sum_{i=1}^S \left| \frac{B_i^{post} - B_i^{pre}}{r_j^{post} - r_j^{pre}} \right|$, where B^{pre} and B^{post} denote the biomass of the species before and after perturbation; r^{pre} and r^{post} denote the production rate of the species before and after perturbation; and S denotes species richness in the food web.

We found that the biomass structure of food webs has little influence on species' total net effect in both empirical and model food webs (**Figs. A6.1 and A6.2**). Consistent relationships between species' traits and their total net effect are present across food webs with varying scaling exponents of species' body mass to biomass (**Tables A6.1 and A6.2**), as well as for total community biomass change (**Fig. A6.3**). These findings suggest that the weak or even inverse correlations between species' traits and keystone-ness (e.g., species' per capita net effect) in food webs with positive scaling largely stemmed from the per capita basis.

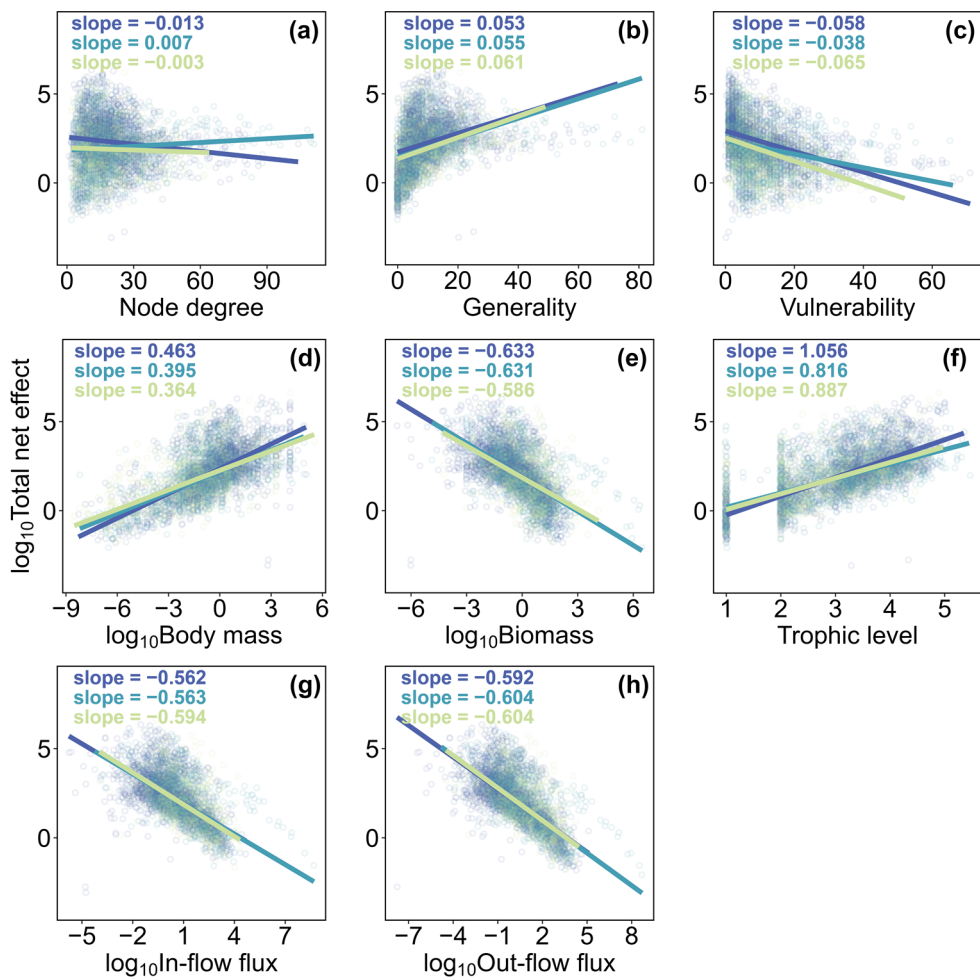


Fig. A6.1 Relationships between species' traits and their total net effect predicted by inverse community matrix in empirical food webs. A random variation (a–c, ± 0.2 ; b–h, ± 0.02) was applied along the x-axis to avoid overlap. Huber regression lines are shown along with their corresponding regression coefficients (slopes). For full statistics see Table A6.1. Colors denote the different groups of empirical food webs (as in

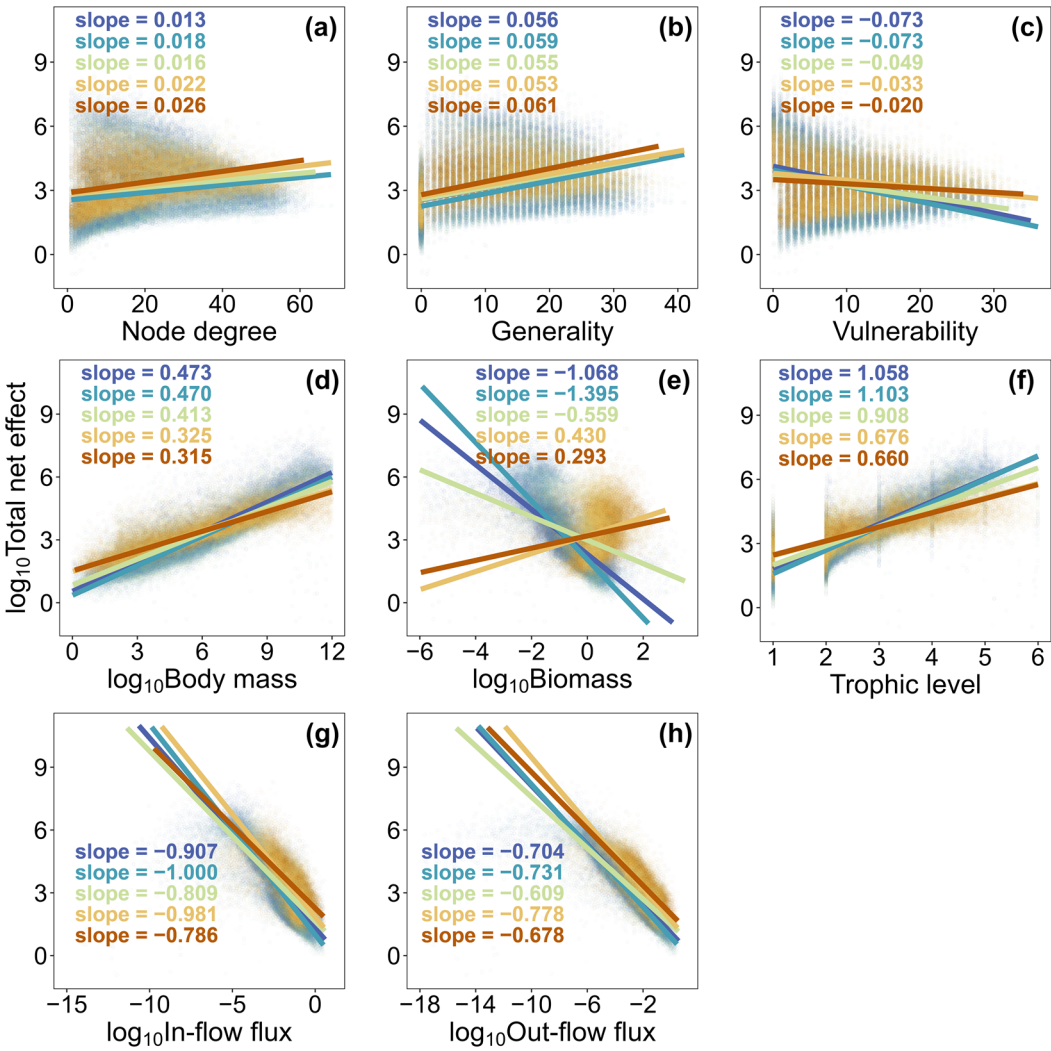
271 Fig. 1b), categorized based on quantiles of the scaling exponent of species' body mass to biomass, with each
 272 group containing an equal number of food webs ($n = 48$).

273

274 **Table A6.1** Huber regression statistics for each group of empirical food webs, analyzing the relationships
 275 between individual species' traits and their total net effect as predicted by the inverse community matrix.
 276 Each group's name is followed by the specific range of the scaling exponent of species' body mass to their
 277 biomass. The 95% confidence intervals for the regression estimates, obtained through bootstrap resampling,
 278 are provided in brackets. Species' total net effect, body mass, biomass, total in-flow flux, and total out-flow
 279 flux were \log_{10} -transformed.

	Empirical food webs		
	Group 1	Group 2	Group 3
Node degree	$[-0.73, -0.35]$ slope = -0.013 $t = -5.449$ ($-0.018, -0.010$)	$[-0.35, -0.23)$ slope = 0.007 $t = 3.023$ ($0.003, 0.011$)	$[-0.23, 0.10)$ slope = -0.003 $t = -1.024$ ($-0.009, 0.002$)
Generality	0.053 $t = 14.379$ ($0.043, 0.064$)	0.055 $t = 16.561$ ($0.046, 0.065$)	0.061 $t = 14.162$ ($0.053, 0.069$)
Vulnerability	-0.058 $t = -20.781$ ($-0.064, -0.051$)	-0.038 $t = -10.396$ ($-0.046, -0.030$)	-0.065 $t = -15.641$ ($-0.072, -0.058$)
Body mass	0.463 $t = 40.786$ ($0.436, 0.492$)	0.395 $t = 31.485$ ($0.370, 0.420$)	0.364 $t = 29.985$ ($0.341, 0.388$)
Biomass	-0.633 $t = -36.965$ ($-0.675, -0.587$)	-0.631 $t = -32.530$ ($-0.686, -0.574$)	-0.586 $t = -23.764$ ($-0.636, -0.533$)
Trophic level	1.056 $t = 40.704$ ($0.998, 1.111$)	0.816 $t = 28.902$ ($0.752, 0.869$)	0.887 $t = 32.754$ ($0.829, 0.945$)
In-flow flux	-0.562 $t = -38.853$ ($-0.596, -0.526$)	-0.563 $t = -33.975$ ($-0.615, -0.510$)	-0.594 $t = -30.659$ ($-0.634, -0.551$)
Out-flow flux	-0.592 $t = -48.300$ ($-0.625, -0.560$)	-0.604 $t = -43.409$ ($-0.645, -0.562$)	-0.604 $t = -38.201$ ($-0.638, -0.569$)

280



281

282 **Fig. A6.2** Relationships between species' traits and their total net effect predicted by inverse community
 283 matrix in model food webs. A random variation (a–c, ± 0.2 ; b–h, ± 0.02) was applied along the x-axis to avoid
 284 overlap. Huber regression lines are shown along with their corresponding regression coefficients (slopes).
 285 For full statistics see Table A6.2. Colors denote the different groups of model food webs (as in Fig. 1b),
 286 categorized based on the scaling exponent of species' body mass to biomass, with each group containing an
 287 equal number of food webs ($n = 559$ or 560).

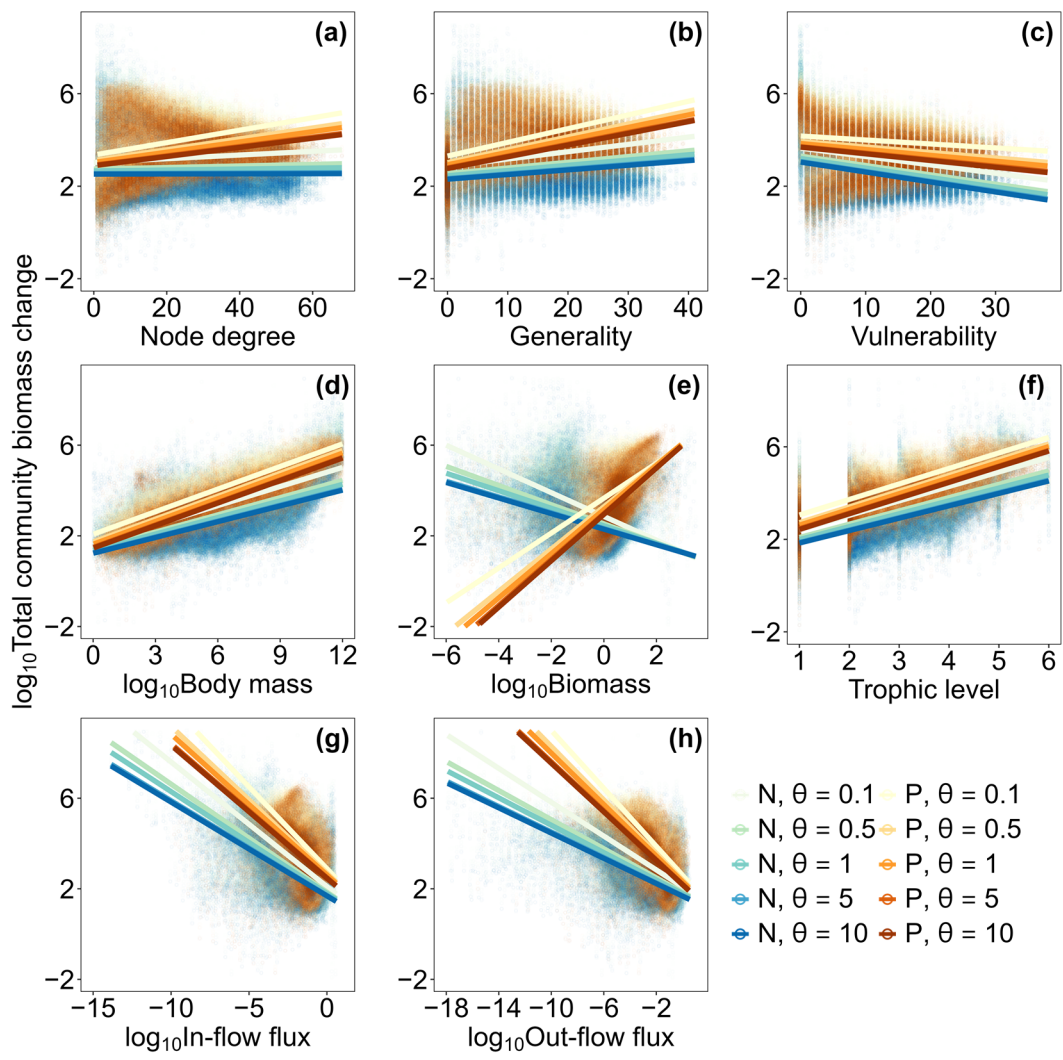
288

289 **Table A6.2** Huber regression statistics for each group of model food webs, examining the relationships
 290 between individual species traits and their total net effect as predicted by the inverse community matrix. Each
 291 group's name is followed by the specific range of the scaling exponent of species' body mass to biomass.
 292 The 95% confidence intervals for the regression estimates, obtained through bootstrap resampling, are
 293 provided in brackets. Species' total net effect, body mass, biomass, total in-flow flux, and total out-flow flux
 294 were log₁₀-transformed.

 Model food webs

	Group 1	Group 2	Group 3	Group 4	Group 5
	[-0.84, -0.28)	[-0.28, -0.24)	[-0.24, 0.02)	[0.02, 0.09)	[0.09, 0.53)
	slope = 0.013	slope = 0.018	slope = 0.016	slope = 0.022	slope = 0.026
Node degree	t = 50.426 (0.012, 0.013)	t = 78.756 (0.017, 0.018)	t = 61.803 (0.016, 0.017)	t = 139.631 (0.021, 0.022)	t = 39.217 (0.025, 0.026)
Generality	slope = 0.056 (0.056, 0.057)	slope = 0.059 (0.059, 0.060)	slope = 0.055 (0.054, 0.055)	slope = 0.053 (0.053, 0.053)	slope = 0.061 (0.061, 0.062)
Vulnerability	slope = -0.073 (-0.074, -0.072)	slope = -0.073 (-0.074, -0.072)	slope = -0.049 (-0.051, -0.048)	slope = -0.033 (-0.033, -0.032)	slope = -0.020 (-0.021, -0.019)
Body mass	slope = 0.473 (0.471, 0.474)	slope = 0.470 (0.468, 0.471)	slope = 0.413 (0.411, 0.414)	slope = 0.325 (0.324, 0.326)	slope = 0.315 (0.313, 0.315)
Biomass	slope = -1.068 (-1.073, -1.063)	slope = -1.395 (-1.401, -1.391)	slope = -0.559 (-0.567, -0.550)	slope = 0.430 (0.412, 0.451)	slope = 0.293 (0.278, 0.305)
Trophic level	slope = 1.058 (1.056, 1.061)	slope = 1.103 (1.100, 1.105)	slope = 0.908 (0.904, 0.911)	slope = 0.676 (0.673, 0.678)	slope = 0.660 (0.657, 0.663)
In-flow flux	slope = -0.907 (-0.912, -0.904)	slope = -1.000 (-1.003, -0.998)	slope = -0.809 (-0.816, -0.801)	slope = -0.981 (-0.986, -0.976)	slope = -0.786 (-0.793, -0.773)
Out-flow flux	slope = -0.704 (-0.706, -0.701)	slope = -0.731 (-0.733, -0.730)	slope = -0.609 (-0.612, -0.606)	slope = -0.778 (-0.781, -0.775)	slope = -0.678 (-0.684, -0.673)

295



296

297 **Fig. A6.3** Relationships between species' traits and their total community biomass change in model food
 298 webs. A random variation (a–c, ± 0.2 ; b–h, ± 0.02) was applied along the x-axis to avoid overlap. Huber
 299 regression lines are shown.

300 **Supplementary Tables**

301 **Table S1** Empirical Ecopath food webs and their ecosystem types. The names of these Ecopath
 302 food webs are the original names from the Ecobase database (<http://ecobase.ecopath.org/>).

ID	Food web	Ecosystem type	ID	Food web	Ecosystem type
1	Alaska, Prince William Sound	Bay/fjord	73	Low Barents sea	Continental shelf
2	Albatross Bay	Bay/fjord	74	Malangen Fjord	Bay/fjord
3	Aleutian Islands	Continental shelf	75	Mauritania	Open ocean
4	Alto Golfo de California	Continental shelf	76	Mid-Atlantic Bight	Continental shelf
5	Antarctic	Open ocean	77	Miramare	Bay/fjord
6	Australia North West Shelf	Continental shelf	78	Moreton Bay Ecosystem	Bay/fjord
7	Azores	Open ocean	79	Morocco	Open ocean
8	Azores archipelago	Continental shelf	80	Mount St Michel Bay	Bay/fjord
9	Baie de Seine	Estuary	81	Narragansett Bay	Estuary
10	Baja California	Continental shelf	82	New Foundland	Open ocean
11	Bamboung	Coastal lagoon	83	Ningaloo	Coral reef
12	Barents Sea	Continental shelf	84	North Aegean	Continental shelf
13	Barnegat Bay	Estuary	85	North Atlantic	Open ocean
14	Bay of Biscay	Continental shelf	86	North Benguela	Upwelling
15	Black Sea	Continental shelf	87	North Brazil	Estuary
16	Bolinao Coral Reef	Coastal lagoon	88	North East Pacific	Continental shelf
17	British Columbia coast	Continental shelf	89	North South of China Sea	Continental shelf
18	Calvi Bay	Bay/fjord	90	Northern Benguela	Upwelling
19	Canada, Grand Banks of Newfoundland	Open ocean	91	Northern British Columbia	Channel/strait
20	Cape Verde	Continental shelf	92	Northern Californian Current	Upwelling
21	Caribbean	Continental shelf	93	Northern Gulf of Mexico	Coastal lagoon
22	Celestun	Coastal lagoon	94	Northern Gulf of St Lawrence	Channel/strait
23	Celestun mangrove	Coastal lagoon	95	Northern Humboldt Current	Upwelling
24	Celtic Sea	Continental shelf	96	Northwest Africa	Open ocean
25	Celtic Sea-Biscay	Continental shelf	97	Orbetello Lagoon	Coastal lagoon
26	Central Atlantic	Open ocean	98	Pagasitikos Gulf	Bay/fjord
27	Central Baltic Sea	Continental shelf	99	Peru	Upwelling
28	Central Chile	Upwelling	100	Port Cros	Continental shelf
29	Central Gulf of California	Channel/strait	101	Port Phillip Bay	Bay/fjord
30	Chantuto-Panzacola	Coastal lagoon	102	Portofino	Coastal lagoon
31	Chesapeake	Bay/fjord	103	Prince William Sound	Bay/fjord
32	Contemporary Alosine	Continental shelf	104	Raja Ampat	Coral reef
33	Cyprus insular shelf	Marine-coastal	105	Restored Alosine Biomass	Continental shelf
34	Danajon Bank	Coral reef	106	Ria Formosa	Coastal lagoon

35	Deep Western Mediterranean sea	Open ocean	107	Santa Pola Bay	fish farm
36	Denmark, Faroe Islands	Open ocean	108	Seagrass and Mangrove Terminos Lagoon	Coastal lagoon
37	East Bass Strait	Continental shelf	109	Sechura Bay	Bay/fjord
38	Eastern Bering Sea	Open ocean	110	Senegambia	Continental shelf
39	Eastern Scotian Shelf	Continental shelf	111	Sierra Leone	Continental shelf
40	Eastern Tropical Pacific	Open ocean	112	Sinaloa sur MEXICO	Continental shelf
41	Eritrea	Coral reef	113	Sonda de Campeche	Continental shelf
42	Falkland Islands	Open ocean	114	South Benguela	Upwelling
43	Galapagos	Coral reef	115	South East Alaska	Continental shelf
44	Galapagos, Floreana rocky reef	Coral reef	116	South Shetlands	Open ocean
45	Georges Bank	Continental shelf	117	South western Gulf of Mexico	Continental shelf
46	Germany, Schlei Fjord	Bay/fjord	118	Southern Brazil	Continental shelf
47	Gironde estuary	Estuary	119	Southern Gulf of St. Lawrence	Continental shelf
48	Golfo Dulce	Bay/fjord	120	Southern New England	Continental shelf
49	Grand Banks of Newfoundland	Open ocean	121	Sri Lanka	Continental shelf
50	Greenland, West Coast	Open ocean	122	Strait of Georgia	Channel/strait
51	Guinea	Continental shelf	123	Tamiahua	Coastal lagoon
52	Gulf of California	Continental shelf	124	Tampa Bay	Estuary
53	Gulf of Carpentaria	Bay/fjord	125	Tasmanian Seamounts Marine Reserve	Open ocean
54	Gulf of Gabes	Continental shelf	126	Tasmanian waters	Continental shelf
55	Gulf of Maine	Continental shelf	127	Terminos Lagoon	Coastal lagoon
56	Gulf of Mexico	Continental shelf	128	Thau	Coastal lagoon
57	Gulf of Nicoya	Estuary	129	Thermaikos Gulf	Bay/fjord
58	Gulf of Salamanca	Upwelling	130	USA, Mid Atlantic Bight	Continental shelf
59	Gulf of Thailande	Continental shelf	131	USA, South Atlantic Continental Shelf	Open ocean
60	Hudson Bay	Bay/fjord	132	Venezuela shelf	Continental shelf
61	Huizache-Caimanero	Coastal lagoon	133	Virgin Islands	Coral reef
62	Humboldt Current	Upwelling	134	West Coast of Peninbsular Malaysia	Continental shelf
63	Iceland	Open ocean	135	West coast of Sabah	Continental shelf
64	Icelandic shelf	Open ocean	136	West Coast Vancouver Island	Continental shelf
65	Independence Bay	Bay/fjord	137	West Florida Shelf	Continental shelf
66	Irish Sea	Continental shelf	138	West Scotland	Continental shelf
67	Jalisco and Colima Coast	Continental shelf	139	West Scotland DeepSea	Open ocean
68	Jurien Bay	Coastal lagoon	140	Western Antarctic Peninsula	Continental shelf
69	Kaloko Honokohau	Coral reef	141	Western Bering Sea	Continental shelf

70	Kuosheng Bay	Bay/fjord	142	Western Channel	Channel/strait
71	Liberia	Continental shelf	143	Western Tropical Pacific	Open ocean
72	Looc Key National Marine Sanctuary	Coral reef	144	Yucatan	Continental shelf

304 **Table S2** Statistics from Huber regressions (using function *rlm* of the *MASS* package in R) for
 305 empirical food webs, assessing the effects of individual species traits, as well as the interaction
 306 between the trait and the species' body mass–biomass scaling exponent of the respective food
 307 web, on species' per capita net effect. The 95% confidence intervals (CIs) for the regression
 308 estimates were obtained through bootstrap resampling. Species' per capita net effect, body mass,
 309 biomass, total in-flow flux, and total out-flow flux were \log_{10} -transformed.

Predictor	Estimate	t	CIs
Species' per capita net effect ~ <i>rlm</i>(Node degree × Scaling exponent)			
Node degree	0.007	3.295	(0.004, 0.010)
Scaling exponent	-0.920	-6.394	(-1.233, -0.630)
Node degree × Scaling exponent	0.024	4.744	(0.017, 0.032)
Species' per capita net effect ~ <i>rlm</i>(Generality × Scaling exponent)			
Generality	0.034	11.234	(0.028, 0.041)
Scaling exponent	-0.469	-3.894	(-0.710, -0.212)
Generality × Scaling exponent	0.034	4.407	(0.016, 0.046)
Species' per capita net effect ~ <i>rlm</i>(Vulnerability × Scaling exponent)			
Vulnerability	-0.017	-5.550	(-0.024, -0.011)
Scaling exponent	-0.773	-6.290	(-1.054, -0.495)
Vulnerability × Scaling exponent	0.016	2.101	(0.002, 0.033)
Species' per capita net effect ~ <i>rlm</i>(Body mass × Scaling exponent)			
Body mass	-0.048	-3.344	(-0.080, -0.016)
Scaling exponent	-0.534	-5.416	(-0.750, -0.320)
Body mass × Scaling exponent	-0.416	-9.525	(-0.519, -0.317)
Species' per capita net effect ~ <i>rlm</i>(Biomass × Scaling exponent)			
Biomass	-0.336	-15.454	(-0.385, -0.283)
Scaling exponent	0.232	2.806	(0.068, 0.394)
Biomass × Scaling exponent	0.003	0.047	(-0.128, 0.150)
Species' per capita net effect ~ <i>rlm</i>(Trophic level × Scaling exponent)			
Trophic level	0.234	7.613	(0.173, 0.307)
Scaling exponent	1.686	6.660	(1.013, 2.294)
Trophic level × Scaling exponent	-0.511	-5.543	(-0.698, -0.307)
Species' per capita net effect ~ <i>rlm</i>(In-flow flux × Scaling exponent)			
In-flow flux	-0.137	-6.134	(-0.188, -0.092)
Scaling exponent	-0.056	-0.578	(-0.230, 0.144)
In-flow flux × Scaling exponent	0.182	2.953	(0.047, 0.305)
Species' per capita net effect ~ <i>rlm</i>(Out-flow flux × Scaling exponent)			
Out-flow flux	-0.142	-7.556	(-0.184, -0.099)
Scaling exponent	0.041	0.467	(-0.127, 0.204)
Out-flow flux × Scaling exponent	0.174	3.315	(0.048, 0.292)

311 **Table S3** Statistics from Huber regressions for each group of empirical food webs, examining
 312 the relationships between individual species' traits and their per capita net effect. Specific
 313 ranges of the scaling exponent of species' body mass to biomass across empirical food webs for
 314 each group were displayed under the group name. The 95% confidence intervals (CIs) for the
 315 regression estimates were obtained through bootstrap resampling, shown in brackets. Species'
 316 per capita net effect, body mass, biomass, total in-flow flux, and total out-flow flux were \log_{10} -
 317 transformed.

	Empirical food webs		
	Group 1 [-0.73, -0.35)	Group 2 [-0.35, -0.23)	Group 3 [-0.23, 0.10)
Node degree	slope = -0.007	slope = 0.004	slope = -0.002
	t = -4.248 (-0.009, -0.004)	t = 2.898 (0.002, 0.007)	t = -0.985 (-0.006, 0.002)
Generality	slope = 0.024	slope = 0.023	slope = 0.020
	t = 9.968 (0.018, 0.032)	t = 10.490 (0.018, 0.029)	t = 6.817 (0.015, 0.026)
Vulnerability	slope = -0.028	slope = -0.013	slope = -0.023
	t = -13.744 (-0.032, -0.024)	t = -5.580 (-0.018, -0.008)	t = -8.181 (-0.028, -0.018)
Body mass	slope = 0.137	slope = 0.074	slope = 0.014
	t = 13.558 (0.114, 0.161)	t = 7.368 (0.050, 0.097)	(t = 1.367 (-0.010, 0.036))
Biomass	slope = -0.354	slope = -0.299	slope = -0.335
	t = -27.521 (-0.386, -0.323)	t = -20.942 (-0.340, -0.254)	t = -18.925 (-0.379, -0.294)
Trophic level	slope = 0.514	slope = 0.326	slope = 0.317
	t = 24.881 (0.465, 0.563)	t = 15.910 (0.288, 0.364)	t = 14.190 (0.269, 0.365)
In-flow flux	slope = -0.238	slope = -0.164	slope = -0.162
	t = -17.870 (-0.270, -0.208)	t = -11.342 (-0.198, -0.128)	t = -9.262 (-0.198, -0.126)
Out-flow flux	slope = -0.233	slope = -0.174	slope = -0.167
	t = -20.630 (-0.260, -0.206)	t = -14.029 (-0.203, -0.144)	t = -11.441 (-0.197, -0.136)

318

319 **Table S4** Statistics from the Huber regressions (using function *rlm* in R) for model food webs,
 320 assessing the effects of individual species traits, as well as the interaction between the trait and
 321 the species' body mass–biomass scaling exponent of the respective food web, on species' per
 322 capita net effect. The 95% confidence intervals (CIs) for the regression estimates were obtained
 323 through bootstrap resampling. Species' per capita net effect, body mass, biomass, total in-flow
 324 flux, and total out-flow flux were \log_{10} -transformed.

Predictor	Estimate	t	CIs
Species' per capita net effect ~ <i>rlm</i>(Node degree × Scaling exponent)			
Node degree	−0.003	−32.900	(−0.003, −0.003)
Scaling exponent	1.112	99.491	(1.076, 1.136)
Node degree × Scaling exponent	−0.045	−98.912	(−0.046, −0.044)
Species' per capita net effect ~ <i>rlm</i>(Generality × Scaling exponent)			
Generality	−0.006	−42.942	(−0.006, −0.005)
Scaling exponent	1.249	150.361	(1.231, 1.265)
Generality × Scaling exponent	−0.104	−173.356	(−0.105, −0.103)
Species' per capita net effect ~ <i>rlm</i>(Vulnerability × Scaling exponent)			
Vulnerability	−0.004	−17.414	(−0.004, −0.003)
Scaling exponent	−0.508	−42.183	(−0.548, −0.468)
Vulnerability × Scaling exponent	0.045	46.404	(0.043, 0.048)
Species' per capita net effect ~ <i>rlm</i>(Body mass × Scaling exponent)			
Body mass	−0.004	−10.998	(−0.005, −0.003)
Scaling exponent	3.195	277.813	(3.167, 3.219)
Body mass × Scaling exponent	−0.569	−312.710	(−0.573, −0.564)
Species' per capita net effect ~ <i>rlm</i>(Biomass × Scaling exponent)			
Biomass	−0.120	−82.025	(−0.125, −0.115)
Scaling exponent	0.856	141.630	(0.840, 0.870)
Biomass × Scaling exponent	1.076	187.123	(1.051, 1.099)
Species' per capita net effect ~ <i>rlm</i>(Trophic level × Scaling exponent)			
Trophic level	−0.014	−17.251	(−0.017, −0.013)
Scaling exponent	3.170	302.818	(3.148, 3.194)
Trophic level × Scaling exponent	−1.377	−349.396	(−1.389, −1.368)
Species' per capita net effect ~ <i>rlm</i>(In-flow flux × Scaling exponent)			
In-flow flux	0.068	57.087	(0.065, 0.071)
Scaling exponent	2.037	230.848	(2.006, 2.070)
In-flow flux × Scaling exponent	1.093	230.006	(1.074, 1.113)
Species' per capita net effect ~ <i>rlm</i>(Out-flow flux × Scaling exponent)			
Out-flow flux	0.076	92.728	(0.074, 0.079)
Scaling exponent	2.546	275.962	(2.513, 2.576)
Out-flow flux × Scaling exponent	0.961	291.923	(0.949, 0.975)

326 **Table S5** Statistics from Huber regressions for each group of model food webs, examining the
 327 relationships between individual species' traits and their per capita net effect. Specific ranges
 328 of the scaling exponent of species' body mass to biomass across model food webs for each
 329 group were displayed under the group name. The 95% confidence intervals (CIs) for the
 330 regression estimates, obtained through bootstrap resampling, are shown in brackets. Species'
 331 per capita net effect, body mass, biomass, total in-flow flux, and total out-flow flux were \log_{10} -
 332 transformed.

Model food webs					
	Group 1 [-0.84, -0.28)	Group 2 [-0.28, -0.24)	Group 3 [-0.24, 0.02)	Group 4 [0.02, 0.09)	Group 5 [0.09, 0.53)
Node degree	slope = 0.011 $t = 98.955$ (0.011, 0.011)	slope = 0.008 $t = 113.962$ (0.008, 0.009)	slope = -0.0002 $t = -1.834$ (-0.0004, 0.000)	slope = -0.006 $t = -111.244$ (-0.006, -0.006)	slope = -0.009 $t = -91.975$ (-0.009, -0.009)
Generality	slope = 0.030 $t = 215.162$ (0.030, 0.030)	slope = 0.020 $t = 227.361$ (0.020, 0.021)	slope = 0.005 $t = 38.541$ (0.005, 0.005)	slope = -0.011 $t = -164.083$ (-0.011, -0.011)	slope = -0.018 $t = -132.558$ (-0.018, -0.018)
Vulnerability	slope = -0.021 $t = -87.035$ (-0.022, -0.021)	slope = -0.016 $t = -94.786$ (-0.016, -0.015)	slope = -0.011 $t = -60.635$ (-0.011, -0.011)	slope = 0.002 $t = 13.724$ (0.001, 0.002)	slope = 0.0001 $t = 0.428$ (-0.0004, 0.0005)
Body mass	slope = 0.187 $t = 514.841$ (0.186, 0.188)	slope = 0.136 $t = 551.514$ (0.135, 0.137)	slope = 0.069 $t = 164.561$ (0.068, 0.070)	slope = -0.043 $t = -171.026$ (-0.044, -0.043)	slope = -0.060 $t = 147.945$ (-0.061, 0.059)
Biomass	slope = -0.473 $t = -498.907$ (-0.476, -0.470)	slope = -0.417 $t = -518.455$ (-0.419, -0.415)	slope = -0.160 $t = -138.216$ (-0.164, -0.154)	slope = -0.052 $t = -38.439$ (-0.057, -0.047)	slope = -0.027 $t = -17.270$ (-0.031, -0.022)
Trophic level	slope = 0.433 $t = 544.753$ (0.431, 0.435)	slope = 0.333 $t = 592.065$ (0.332, 0.335)	slope = 0.164 $t = 171.560$ (0.161, 0.167)	slope = -0.109 $t = -199.262$ (-0.110, -0.107)	slope = -0.156 $t = -175.847$ (-0.158, -0.154)
In-flow flux	slope = -0.260 $t = -280.278$ (-0.263, -0.256)	slope = -0.229 $t = -351.708$ (-0.231, -0.227)	slope = -0.082 $t = -95.578$ (-0.086, -0.080)	slope = 0.162 $t = 206.936$ (0.159, 0.164)	slope = 0.195 $t = 171.478$ (0.192, 0.198)
Out-flow flux	slope = -0.226 $t = -372.603$ (-0.228, -0.223)	slope = -0.171 $t = -403.036$ (-0.173, -0.170)	slope = -0.057 $t = -88.582$ (-0.059, -0.055)	slope = 0.149 $t = 278.351$ (0.148, 0.151)	slope = 0.190 $t = 228.948$ (0.187, 0.192)

333

334 **Table S6** Interquartile ranges of Spearman rank correlation coefficient between species' per
 335 capita net effect and their per capita community biomass change across model food webs with
 336 either negative or positive species' body mass–biomass scaling. Here, species-specific press
 337 perturbations were applied by multiplying the pre-perturbation production gain of the perturbed
 338 species by a factor of $1/(1+\theta)$, where θ denotes the perturbation size.

θ	Model food webs with negative species' body mass–biomass scaling	Model food webs with positive species' body mass–biomass scaling
0.1	(0.62, 0.80)	(0.33, 0.59)
0.5	(0.70, 0.88)	(0.41, 0.69)
1	(0.73, 0.89)	(0.38, 0.67)
5	(0.83, 0.89)	(0.32, 0.62)
10	(0.72, 0.89)	(0.32, 0.62)

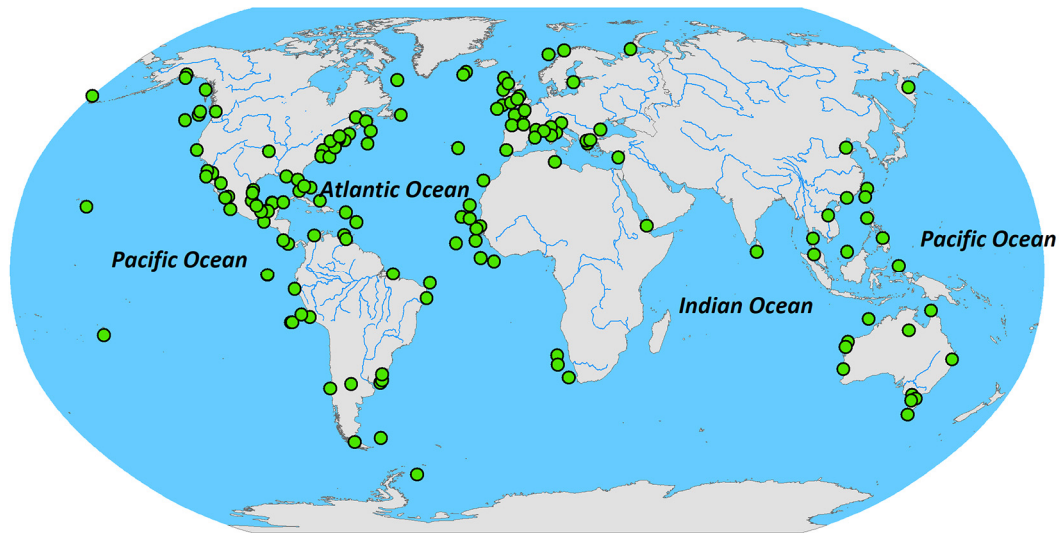
339

340 **Table S7** Statistics from the Huber regressions examining the relationships between individual species' traits and their per capita community biomass
 341 change resulted from species-specific press perturbations in model food webs, differentiated by: (top) negative and (bottom) positive species' body mass–
 342 biomass scaling. Here, species-specific press perturbations were applied by multiplying the pre-perturbation production gain of the perturbed species by
 343 a factor of $1/(1+\theta)$, where θ denotes the perturbation size. Species' per capita community biomass change, biomass, in-flow flux, and out-flow flux were
 344 log₁₀-transformed. The 95% confidence intervals (CIs) for the regression estimates, obtained through bootstrap resampling, are shown in brackets.

Model food webs with negative species' body mass–biomass scaling								
θ	Node degree	Generality	Vulnerability	Body mass	Biomass	Trophic level	In-flow flux	Out-flow flux
0.1	slope	0.017	0.036	−0.010	0.197	−0.750	0.463	−0.422
	t	79.986	132.428	−22.452	223.675	−397.732	232.430	−251.056
	CIs	(0.016, 0.017)	(0.036, 0.037)	(−0.011, −0.009)	(0.195, 0.200)	(−0.756, −0.746)	(0.459, 0.469)	(−0.426, −0.416)
0.5	slope	0.011	0.030	−0.018	0.190	−0.722	0.458	−0.418
	t	60.485	122.835	−46.393	255.180	−445.747	278.476	−290.089
	CIs	(0.011, 0.012)	(0.029, 0.030)	(−0.019, −0.017)	(0.188, 0.192)	(−0.727, −0.718)	(0.454, 0.462)	(−0.422, −0.414)
1	slope	0.010	0.028	−0.020	0.186	−0.708	0.453	−0.414
	t	54.736	118.895	−52.514	258.191	−445.895	286.037	−296.652
	CIs	(0.010, 0.010)	(0.028, 0.029)	(−0.021, −0.019)	(0.184, 0.188)	(−0.713, −0.704)	(0.449, 0.457)	(−0.418, −0.409)
5	slope	0.009	0.028	−0.022	0.186	−0.701	0.456	−0.415
	t	48.645	114.758	−58.832	258.835	−437.677	292.697	−299.821
	CIs	(0.009, 0.009)	(0.027, 0.028)	(−0.023, −0.022)	(0.184, 0.187)	(−0.706, −0.697)	(0.452, 0.460)	(−0.419, −0.410)
10	slope	0.009	0.028	−0.023	0.186	−0.700	0.458	−0.415
	t	48.082	114.407	−59.493	258.987	−435.253	293.628	−299.494
	CIs	(0.009, 0.009)	(0.027, 0.028)	(−0.024, −0.022)	(0.184, 0.188)	(−0.705, −0.695)	(0.453, 0.462)	(−0.420, −0.411)
Model food webs with positive species' body mass–biomass scaling								
0.1	slope	−0.003	−0.011	0.010	−0.098	−0.652	−0.178	0.047
	t	−22.322	−53.961	32.780	−148.620	−245.373	−116.197	21.232

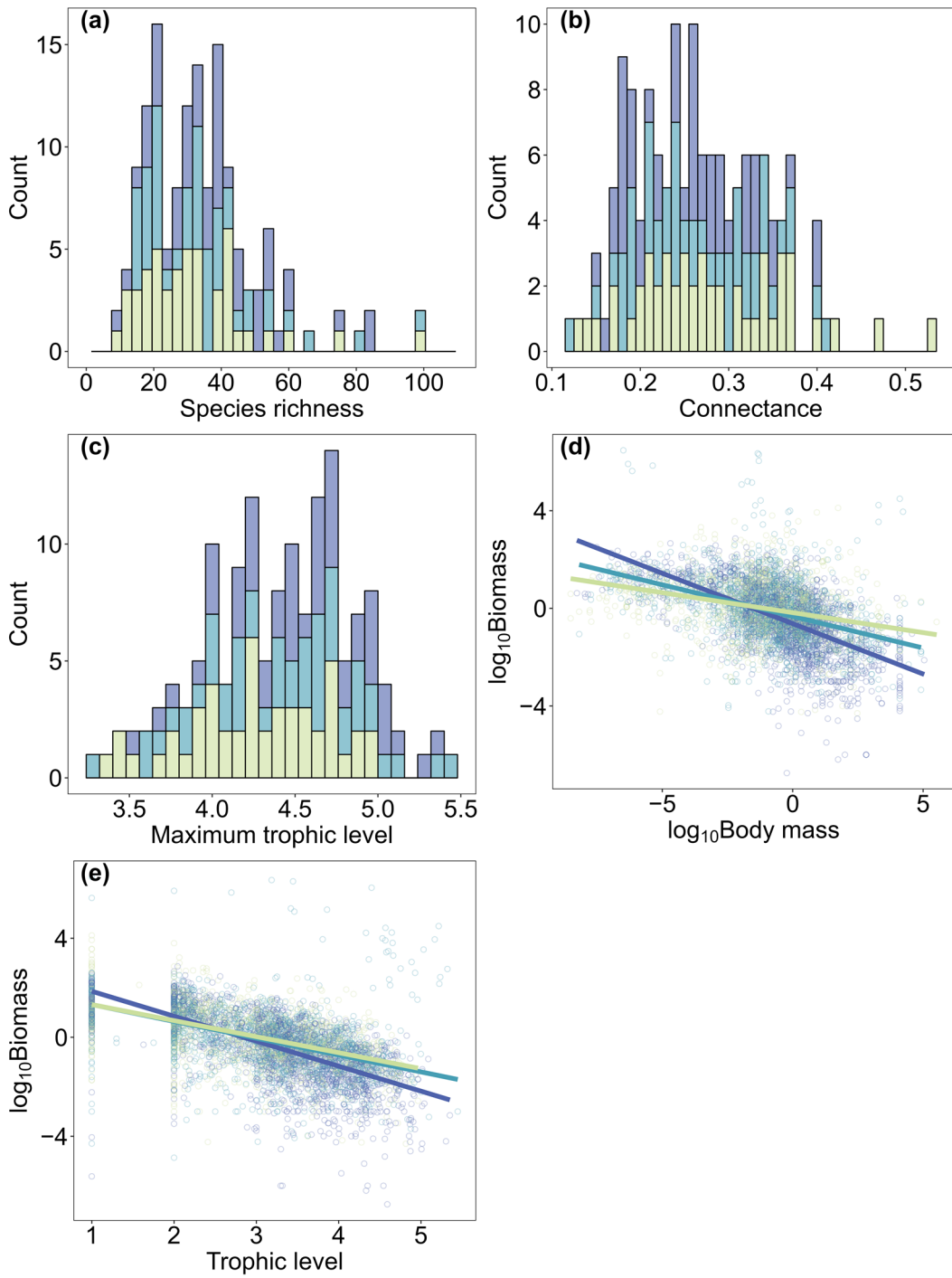
	CIs	(-0.004, -0.003)	(-0.012, -0.011)	(0.009, 0.010)	(-0.100, -0.097)	(-0.660, -0.641)	(-0.182, -0.174)	(0.037, 0.054)	(0.061, 0.072)
0.5	slope	-0.006	-0.013	0.004	-0.084	-0.582	-0.155	0.067	0.080
	t	-48.196	-77.271	14.987	-167.827	-279.195	-133.839	39.430	63.302
1	CIs	(-0.006, -0.006)	(-0.013, -0.012)	(0.003, 0.004)	(-0.085, -0.083)	(-0.595, -0.571)	(-0.158, -0.153)	(0.062, 0.074)	(0.076, 0.085)
	slope	-0.006	-0.012	0.002	-0.080	-0.563	-0.147	0.057	0.072
5	t	-53.458	-80.691	9.536	-168.204	-284.069	-133.368	35.154	59.532
	CIs	(-0.006, -0.006)	(-0.013, -0.012)	(0.002, 0.003)	(-0.081, -0.078)	(-0.573, -0.553)	(-0.150, -0.145)	(0.050, 0.063)	(0.068, 0.077)
10	slope	-0.006	-0.012	0.001	-0.075	-0.538	-0.135	0.041	0.058
	t	-53.447	-78.010	6.056	-167.119	-283.592	-128.533	26.124	49.690
	CIs	(-0.006, -0.006)	(-0.012, -0.011)	(0.001, 0.002)	(-0.076, -0.074)	(-0.546, -0.530)	(-0.137, -0.132)	(0.035, 0.046)	(0.053, 0.062)
	slope	-0.006	-0.011	0.001	-0.074	-0.532	-0.132	0.039	0.057
	t	-53.272	-77.303	5.333	-165.922	-281.894	-126.561	25.259	48.751
	CIs	(-0.006, -0.006)	(-0.012, -0.011)	(0.001, 0.002)	(-0.075, -0.073)	(-0.542, -0.521)	(-0.135, -0.130)	(0.032, 0.046)	(0.053, 0.061)

346 **Supplementary Figures**



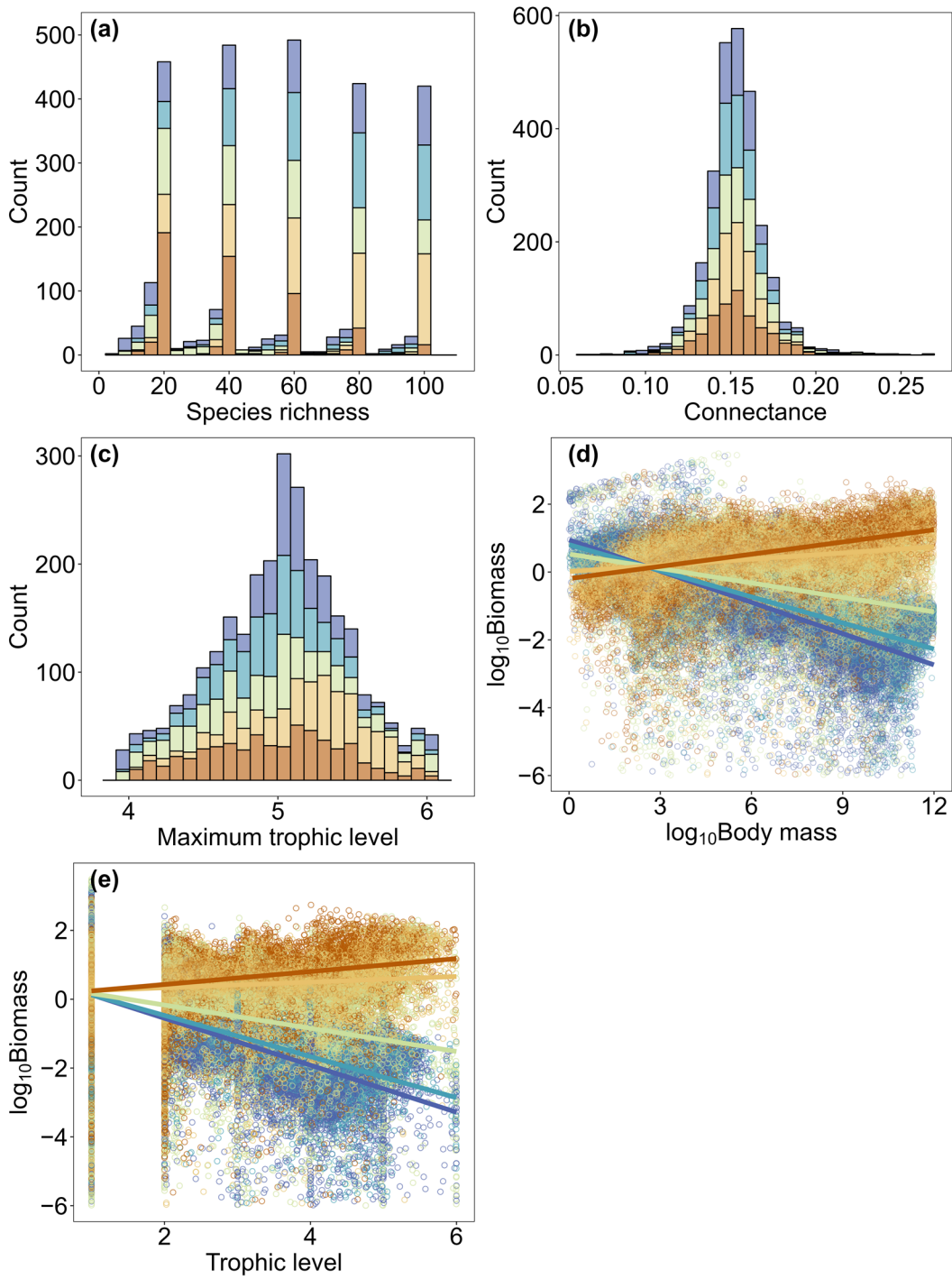
347

348 **Fig. S1** Map of the collected 144 empirical Ecopath food webs. For names of these empirical
349 food webs see Table S1.



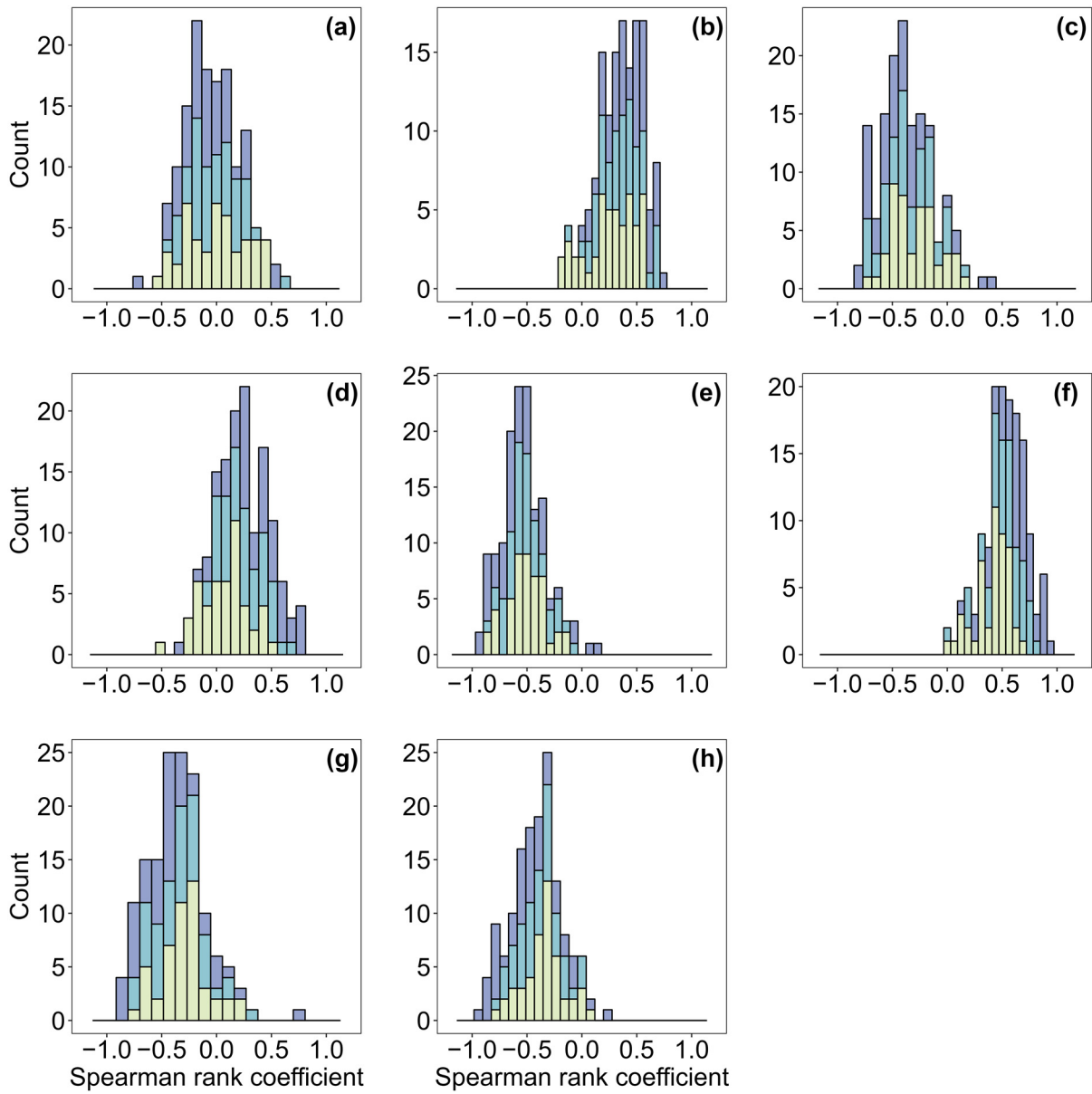
350

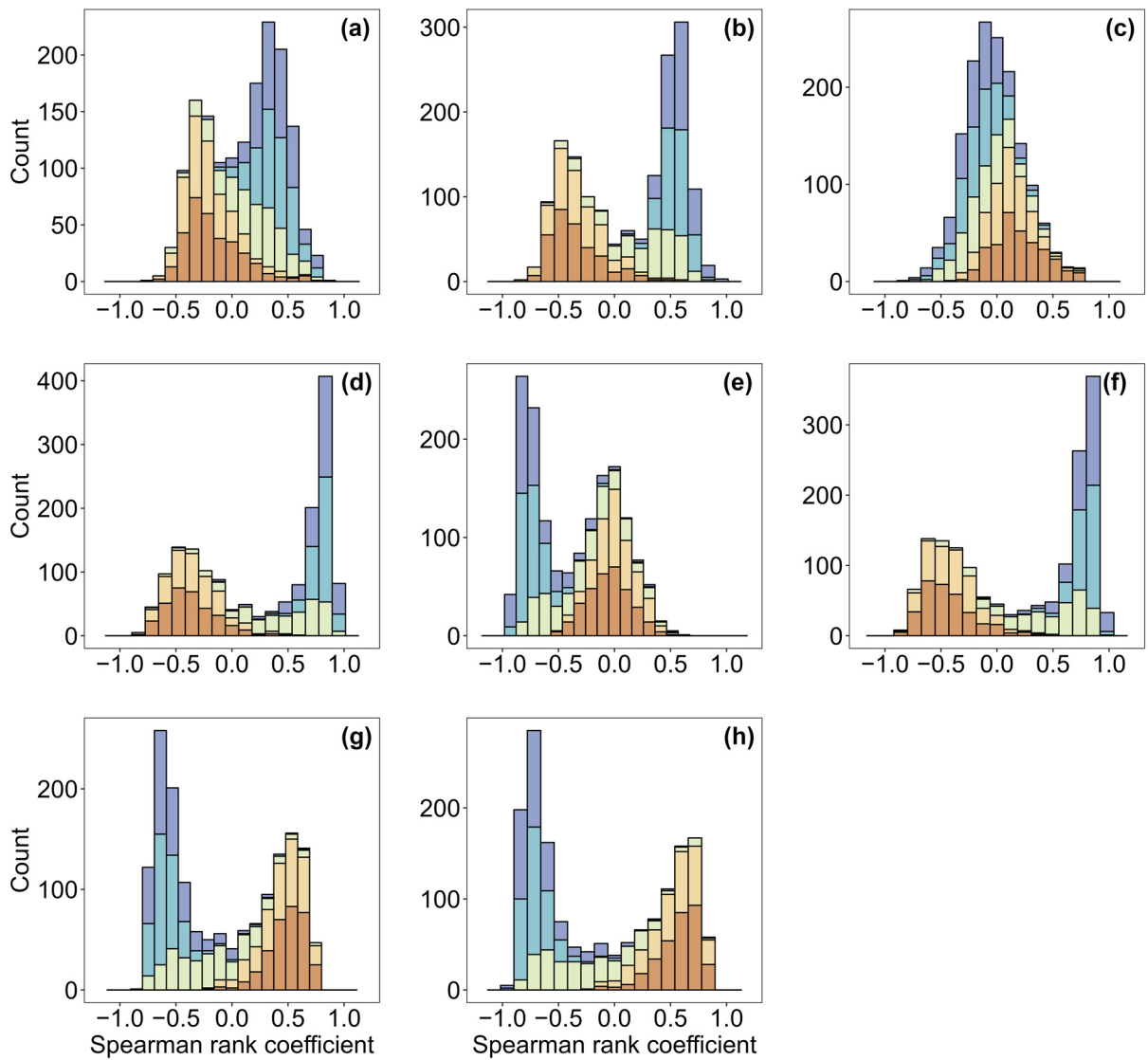
351 **Fig. S2** Characteristics in the 144 empirical food webs. (a–c) Histogram distributions of species
 352 richness, connectance, and consumers' maximum trophic level across these food webs. Colors
 353 denote the different groups of empirical food webs (as in Fig. 1b), categorized based on
 354 quantiles of the scaling exponent of species' body mass to biomass, ranging from −0.73 to 0.10,
 355 with each group containing an equal number of food webs ($n = 48$). (d–e) Relationships between
 356 species' biomass and their body mass and trophic level. Huber regression for each group of
 357 empirical food webs is shown.



358
359
360
361
362
363
364
365

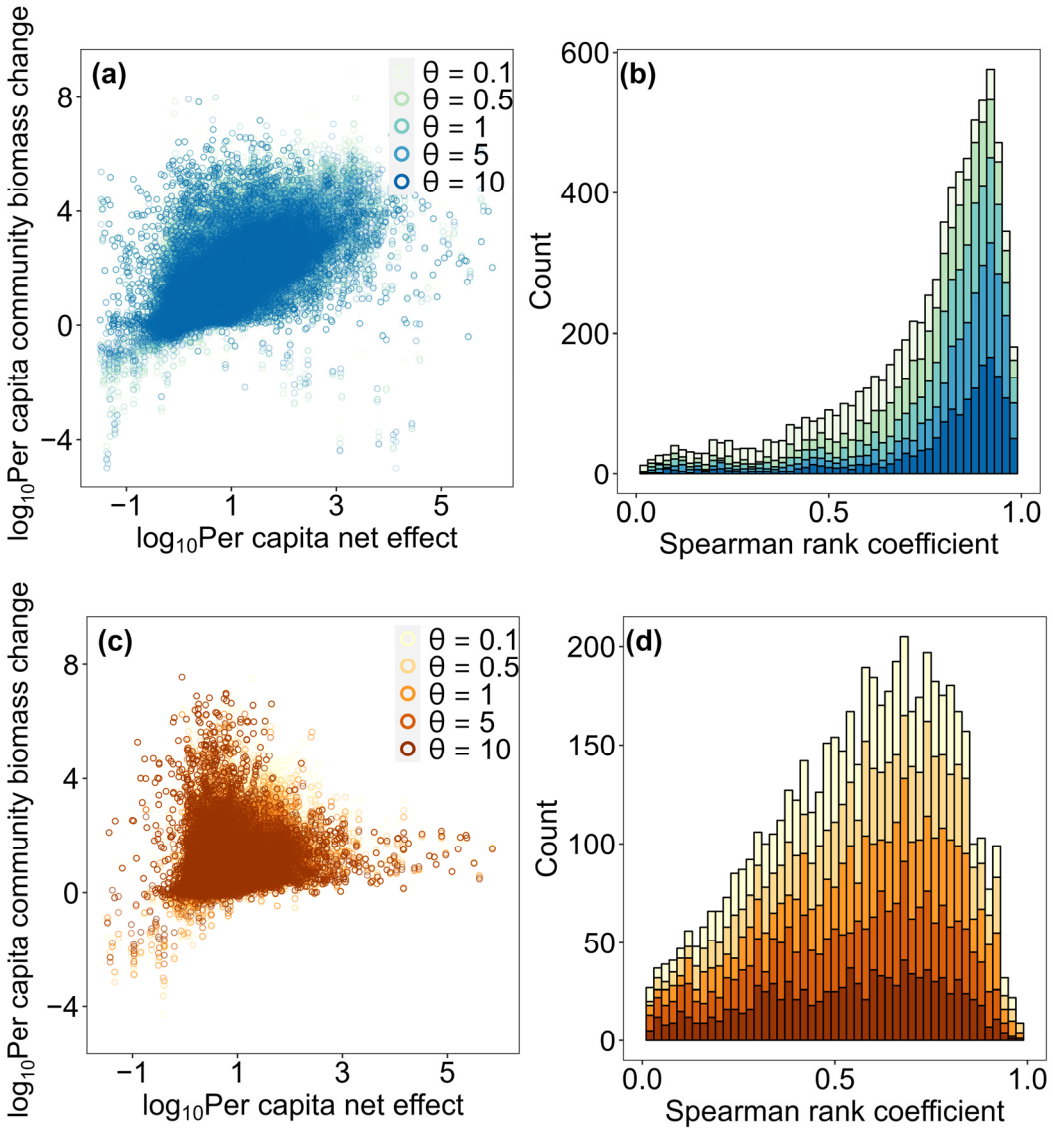
Fig. S3 Characteristics in the model food webs. (a–c) Histogram distributions of species richness, connectance, and consumers' maximum trophic level across 2,799 model food webs. Colors denote the different groups of model food webs (as in Fig. 1b), which were categorized based on the scaling exponent of species' body mass to biomass, ranging from -0.71 to 0.53 , with each group containing an equal number of food webs ($n = 559$ or 560). (d–e) Huber regressions between species' biomass and their body mass and trophic level across the different groups of model food webs.





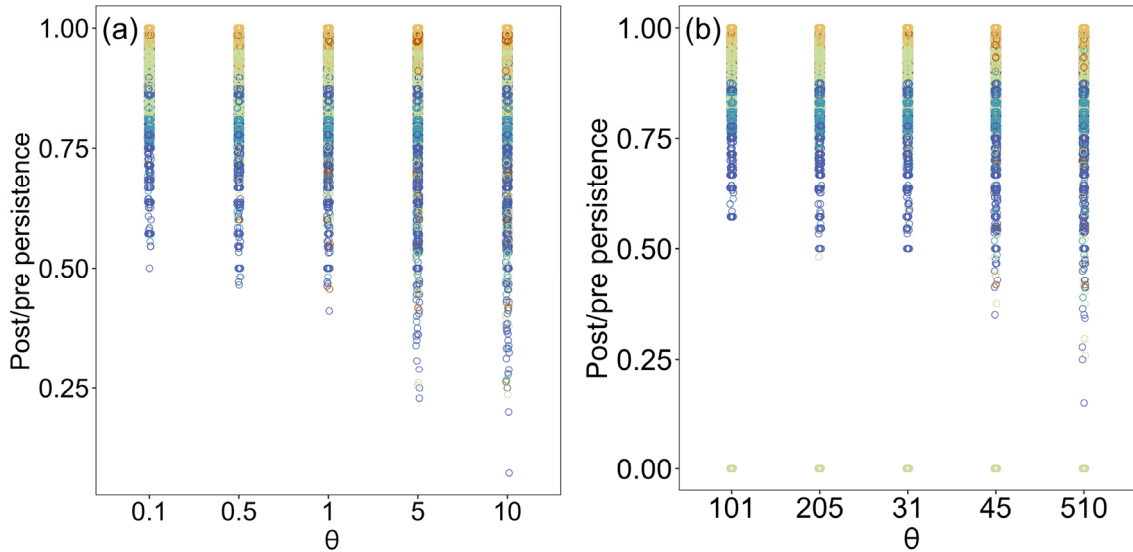
374

375 **Fig. S5** Histogram distributions of Spearman rank correlation coefficients between species' 376 traits and their per capita net effect across model food webs. Corresponding traits are in order 377 of Fig. 3: (a) node degree; (b) generality; (c) vulnerability; (d) $\log_{10}(\text{body mass})$; (e) 378 $\log_{10}(\text{biomass})$; (f) trophic level; (g) $\log_{10}(\text{in-flow flux})$; (h) $\log_{10}(\text{out-flow flux})$. Colors denote 379 the different groups of model food webs (as in Fig. 1b), which were categorized based on the 380 scaling exponent of species' body mass to biomass, ranging from -0.71 to 0.53, with each group 381 containing an equal number of food webs ($n = 559$ or 560).



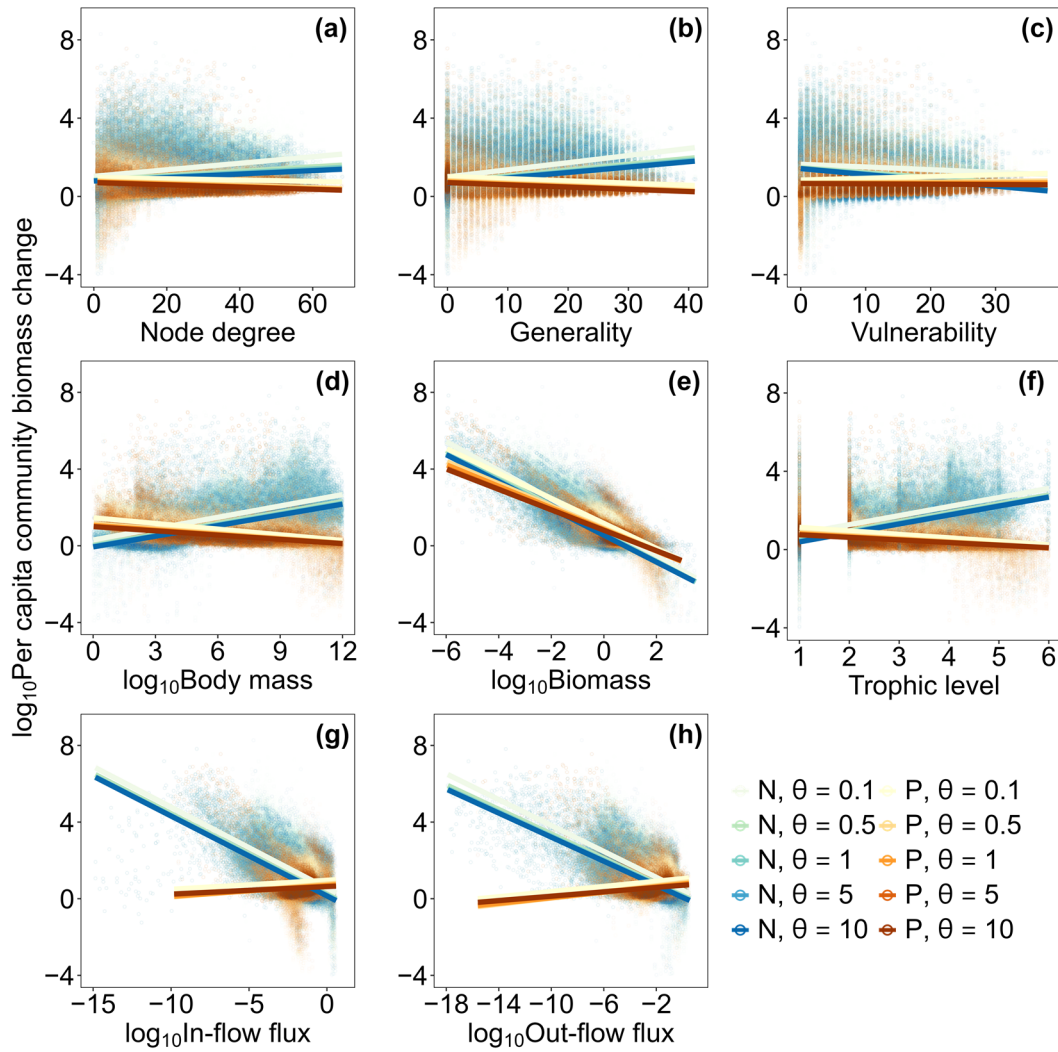
382

383 **Fig. S6** Relationships between species' per capita net effect and their corresponding per capita
 384 community biomass change in model food webs, differentiated by food webs with (a, b)
 385 negative and (c, d) positive species' body mass–biomass scaling. Species per capita net effect
 386 was derived from the normalized inverse community matrix. Species' per capita community
 387 biomass change was calculated after performing species-specific press perturbations by
 388 multiplying the pre-perturbation basal maintenance loss of the perturbed species by a factor of
 389 $1+\theta$, where θ values of 0.1, 0.5, 1, 5, and 10 are represented in different colors. (b, d) Histogram
 390 distributions of the Spearman rank correlation coefficient between the per capita net effect and
 391 the per capita community biomass change of species within each model food web.



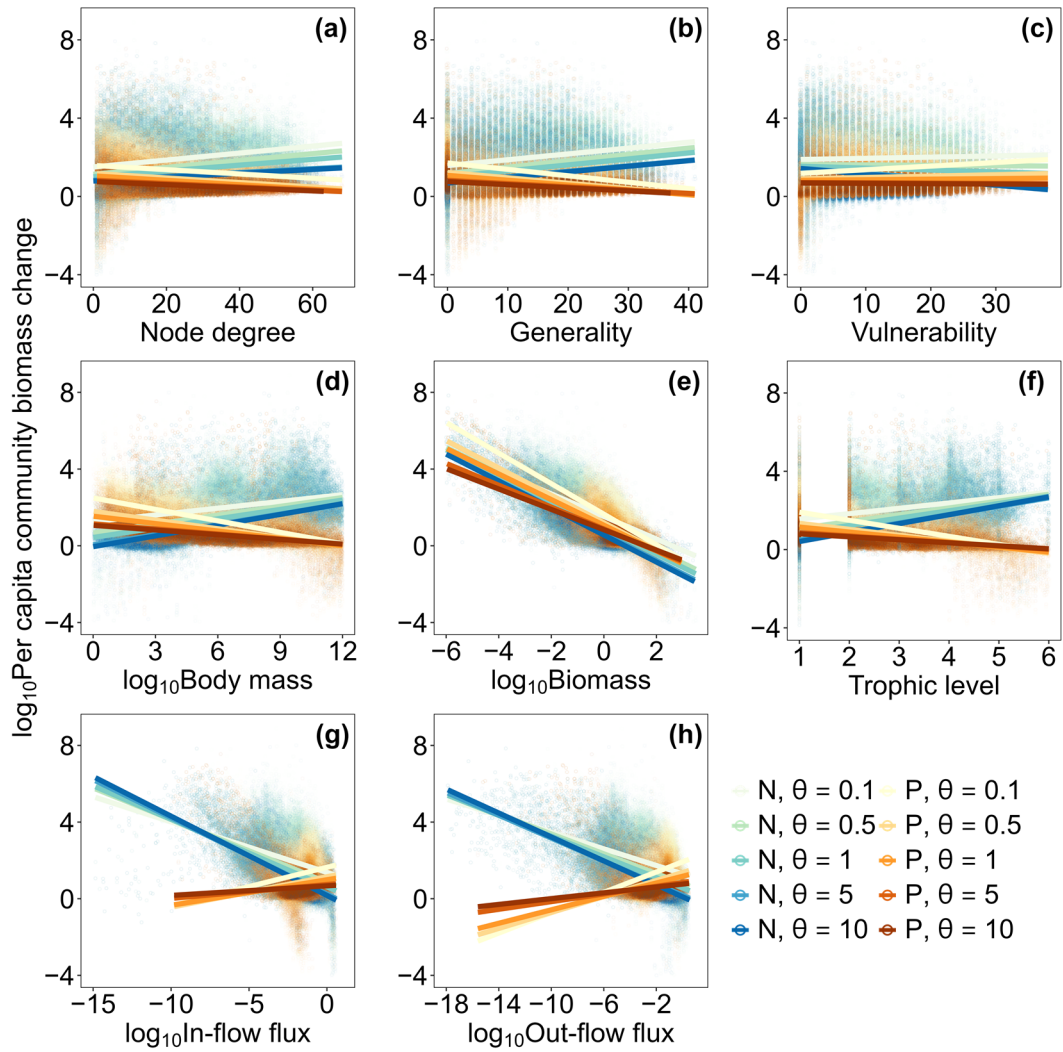
392

393 **Fig. S7** Post/pre-species persistence of model food webs after each species-specific press
 394 perturbation across different sizes of press perturbations (θ). (a) Species-specific press
 395 perturbations were applied by multiplying the pre-perturbation production gain of the perturbed
 396 species by a factor of $1/(1+\theta)$. (b) Species-specific press perturbations were applied by
 397 multiplying the pre-perturbation basal maintenance loss of the perturbed species by a factor of
 398 $1+\theta$. Colors denote the five groups of model food webs characterized by their scaling exponent
 399 of species' body mass to biomass (as in Fig. 1b).



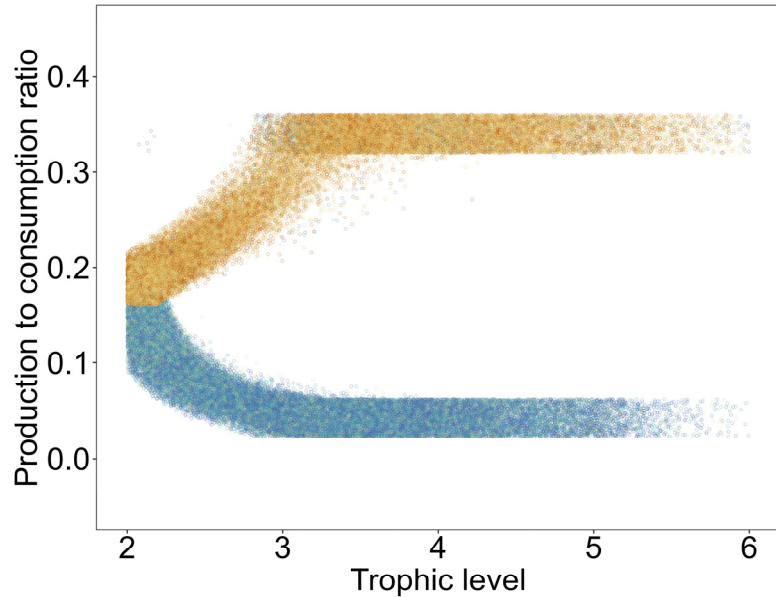
400

401 **Fig. S8** Relationships between species' traits and their per capita community biomass change
 402 calculated by performing species-specific press perturbations in model food webs. Species-
 403 specific press perturbations were applied by multiplying the pre-perturbation production gain
 404 of the perturbed species by a factor of $1/(1+\theta)$, where θ values of 0.1, 0.5, 1, 5, and 10 are
 405 represented in different colors. N and P in the legend refer to the model food web exhibiting
 406 negative and positive species' body mass–biomass scaling, respectively. Huber regression lines
 407 are shown, and detailed statistics of the Huber regressions are provided in Table S7.



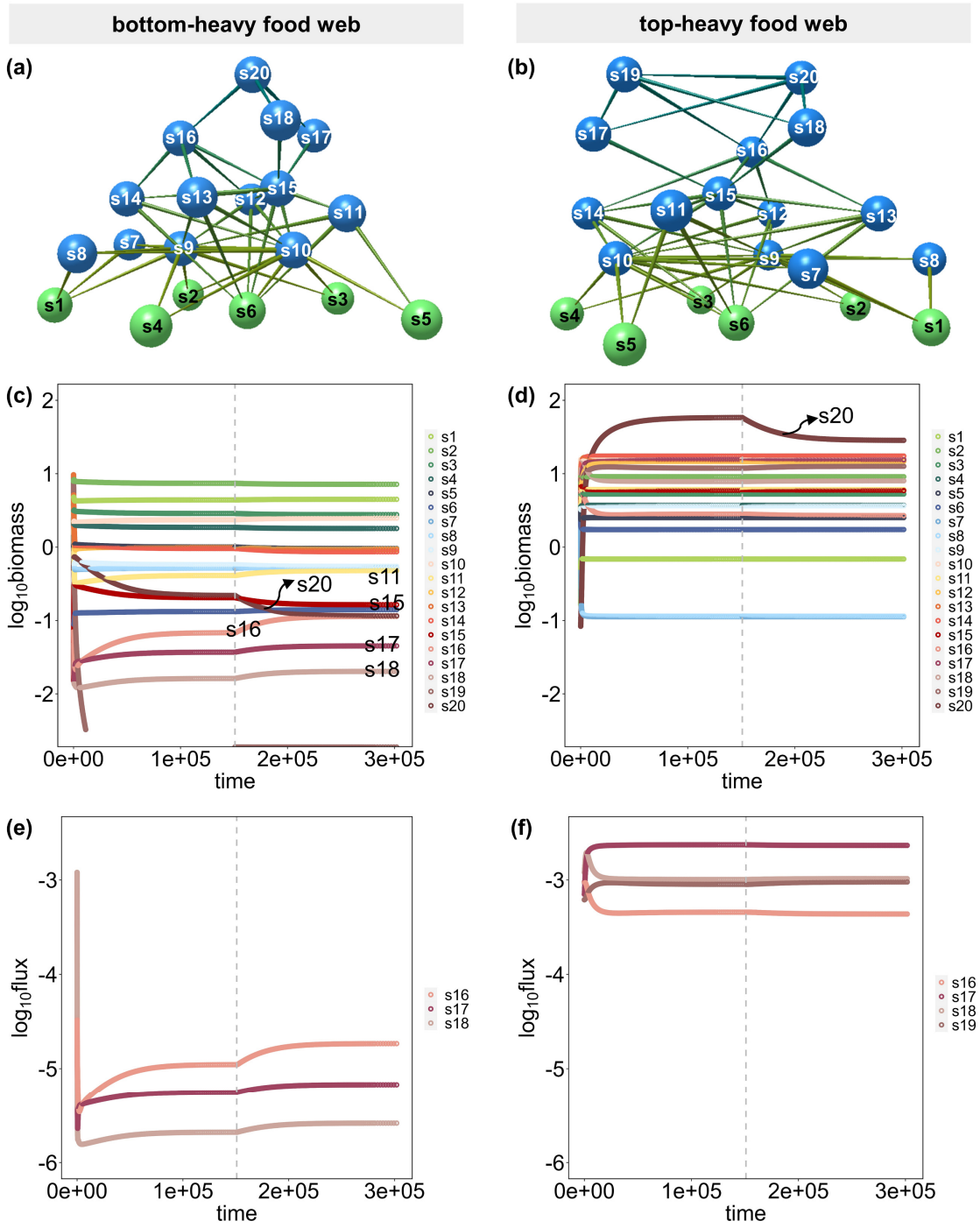
408

409 **Fig. S9** Relationships between species' traits and their per capita community biomass change
 410 calculated by performing species-specific press perturbations in model food webs. Here,
 411 species-specific press perturbations were applied by multiplying the pre-perturbation basal
 412 maintenance loss of the perturbed species by a factor of $1+\theta$, where θ values of 0.1, 0.5, 1,
 413 5, and 10 are represented in different colors. N and P refer to the model food web exhibiting
 414 negative and positive species' body mass–biomass scaling, respectively.



415

416 **Fig. S10** Species' production to consumption ratios across their trophic levels in model food
417 webs. Colors denote the five groups of model food webs characterized by their scaling exponent
418 of species' body mass to biomass (as in Fig. 1b).



419

420 **Fig. S11** Example of a bottom-heavy (left) and a top-heavy (right) model food web responding
421 to species-specific press perturbation. (a, b) Green and blue nodes depict basal species and
422 consumers, respectively, with the vertical level of each node indicating its trophic position. (c,
423 d) Biomass dynamics before and after a perturbation applied to species s_{20} , reducing its
424 production gain by 66.7%, implemented at the time step marked by the dashed line. (e, f)
425 Dynamics of the total flux leaving a species, consisting of the loss to consumption by its
426 predators and its basal maintenance loss. Only the prey species of the perturbed s_{20} are shown.

427 **Supplementary References**

- 428 Anderson, T.R. (1992). Modelling the influence of food C:N ratio, and respiration on growth
429 and nitrogen excretion in marine zooplankton and bacteria. *J. Plankton Res.*, 14, 1645–
430 1671.
- 431 Bender, E.A., Case, T.J. & Gilpin, M.E. (1984). Perturbation experiments in community
432 ecology: Theory and practice. *Ecology*, 65, 1–13.
- 433 Berg, S., Christianou, M., Jonsson, T. & Ebenman, B. (2011). Using sensitivity analysis to
434 identify keystone species and keystone links in size-based food webs. *Oikos*, 120, 510–
435 519.
- 436 Boit, A., Martinez, N.D., Williams, R.J. & Gaedke, U. (2012). Mechanistic theory and
437 modelling of complex food-web dynamics in Lake Constance. *Ecol. Lett.*, 15, 594–602.
- 438 Brose, U., Williams, R. J., & Martinez, N.D. (2006). Allometric scaling enhances stability in
439 complex food webs. *Ecol. Lett.*, 9, 1228–1236.
- 440 Brown, J.H., Gillooly, J.F., Allen, A.P., Savage, V.M., & West, G.B. (2004). Toward a metabolic
441 theory of ecology. *Ecology*, 85, 1771–1789.
- 442 de Ruiter, P.C., Neutel, A.-M. & Moore, J.C. (1995). Energetics, patterns of interaction strengths,
443 and stability in real ecosystems. *Science*, 269, 1257–1260.
- 444 Gessaman, J.A. (1973). *Methods of estimating the energy cost of free existence*. In: Logan UT
445 (ed) Ecological energetics of homeotherms. Utah State University Press, Logan, Utah, 3–
446 31.
- 447 Heal, O.W., & MacLean, S.F. (1975). *Comparative productivity in ecosystems-secondary
448 productivity*. In: Van Dobben WH, Lowe-McConnell RH (eds) Unifying concepts in
449 ecology. Springer, Dordrecht, 89–108.
- 450 Iles, A.C., & Novak, M. (2016). Complexity increases predictability in allometrically
451 constrained food webs. *Am. Nat.*, 188, 87–98.
- 452 Kath, N.J., Boit, A., Guill, C. & Gaedke, U. (2018). Accounting for activity respiration results
453 in realistic trophic transfer efficiencies in allometric trophic network (ATN) models. *Theor.
454 Ecol.*, 11, 453–463.
- 455 Koslicki, D., & Novak, M. (2018). Exact probabilities for the indeterminacy of complex
456 networks as perceived through press perturbations. *J. Math. Biol.*, 76, 877–909.
- 457 Martinez, N.D. (2020). Allometric trophic networks from individuals to socio-ecosystems:
458 Consumer–resource theory of the ecological elephant in the room. *Front. Ecol. Evol.*, 8,
459 92.
- 460 Montoya, J.M., Woodward, G., Emmerson, M.C. & Solé, R.V. (2009). Press perturbations and
461 indirect effects in real food webs. *Ecology*, 90, 2426–2433.
- 462 Nakajima H. (1992). Sensitivity and stability of flow networks. *Ecol. Model.*, 62, 123–133.
- 463 Neutel, A.-M., Heesterbeek, J.A.P. & de Ruiter, P.C. (2002). Stability in real food webs: weak
464 links in long loops. *Science*, 296, 1120–1123.
- 465 Novak, M., Wootton, J.T., Doak, D.F., Emmerson, M., Estes, J.A., & Tinker, M.T. (2011).
466 Predicting community responses to perturbations in the face of imperfect knowledge and

- 467 network complexity. *Ecology*, 92, 836–846.
- 468 Novak, M., Yeakel, J.D., Noble, A.E., Doak, D.F., Emmerson, M., Estes, J.A., et al. (2016).
469 Characterizing species interactions to understand press perturbations: what is the
470 community matrix? *Annu. Rev. Ecol. Evol. Syst.*, 47, 409–432.
- 471 Rall, B.C., Brose, U., Hartvig, M., Kalinkat, G., Schwarzmüller, F., Vucic-Pestic, O., et al.
472 (2012). Universal temperature and body-mass scaling of feeding rates. *Philos. T. R. Soc.
B.*, 367, 2923–2934.
- 473 Ryser, R., Hirt, M.R., Häussler, J., Gravel, D. & Brose, U. (2021). Landscape heterogeneity
474 buffers biodiversity of simulated meta-food-webs under global change through rescue and
475 drainage effects. *Nat. Commun.*, 12, 4716.
- 476 Schneider, F.D., Brose, U., Rall, B.C. & Guill, C. (2016). Animal diversity and ecosystem
477 functioning in dynamic food webs. *Nat. Commun.*, 7, 12718.
- 478 Yodzis, P. & Innes, S. (1992). Body size and consumer-resource dynamics. *Am. Nat.*, 139,
479 1151–1175.
- 480 Yodzis, P. (1988). The indeterminacy of ecological interactions as perceived through
481 perturbation experiments. *Ecology*, 69, 508–515.
- 483